Functional activity and connectivity patterns between Barrington's nucleus and the pons using 7T fMRI scans

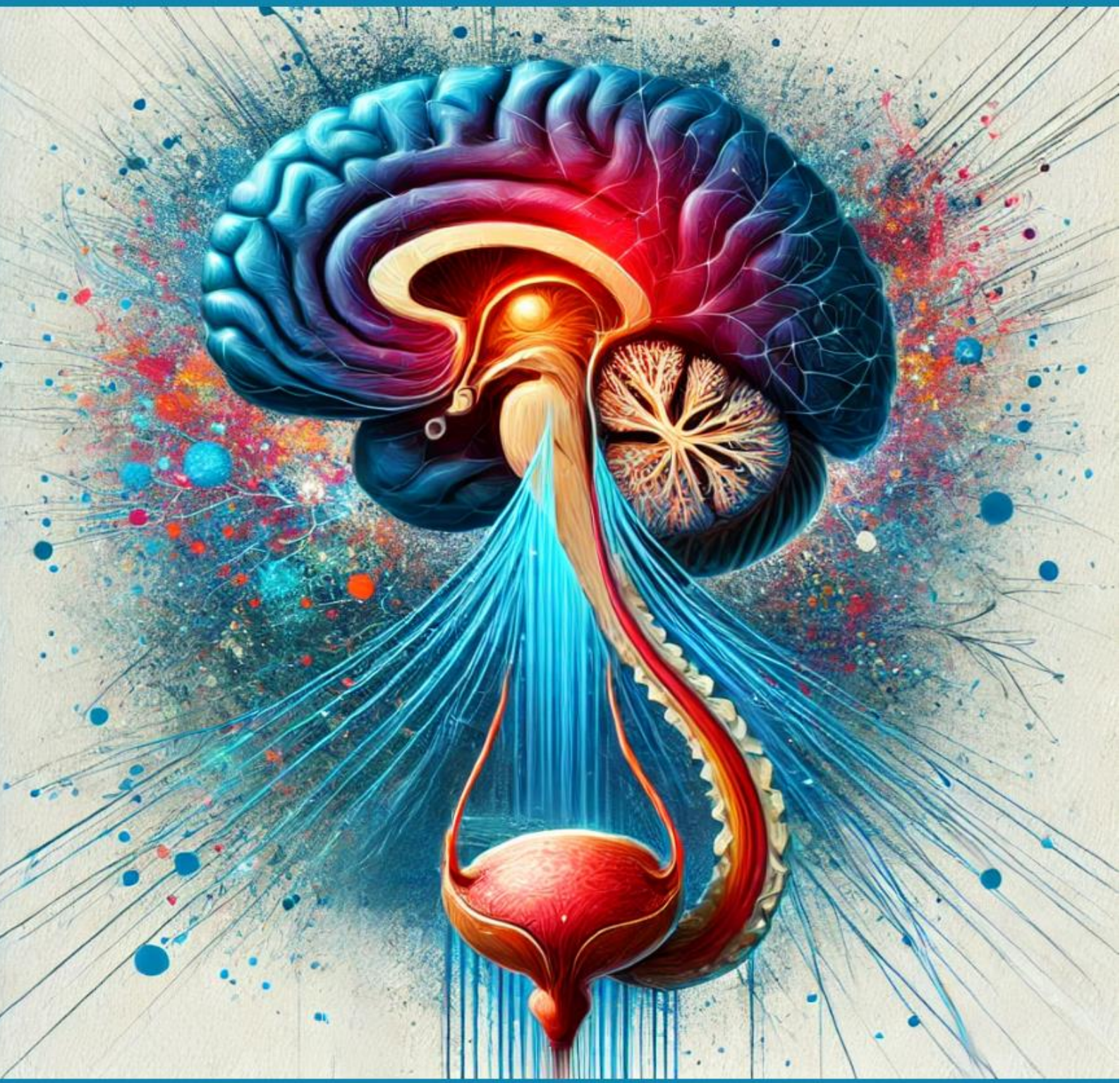

Armelle Knops

Universiteit Leiden
The Netherlands

TU Delft
Delft University of Technology

Erasmus University Rotterdam

Maastricht UMC+

Universiteit Leiden

TU Delft Delft University of Technology

ERASMUS UNIVERSITEIT ROTTERDAM

Functional activity and connectivity patterns between Barrington's nucleus and the pons using 7T fMRI scans

Armelle Knops

Student number : 5184428

04-09-2024

Thesis in partial fulfilment of the requirements for the joint degree of Master of Science in

Technical Medicine

Leiden University ; Delft University of Technology ; Erasmus University Rotterdam

Master thesis project (TM30004 ; 35 ECTS)

29-01-24 TM30004 – 04-09-24 TM30004

Supervisor(s):
Prof. dr. Gommert van Koeveringe | MUMC+
Dr. Job van den Hurk | Scannexus
Drs. Martijn Smits | MUMC+
Prof. dr. Bertil Blok | Erasmus MC

Thesis committee members:
Dr. Abraham Schoe | LUMC (chair)
Prof. dr. Gommert van Koeveringe | MUMC+
Dr. Job van den Hurk | Scannexus
Prof. dr. Bertil Blok | Erasmus MC

...

Universiteit Leiden

TU Delft Delft University of Technology

Erasmus Universiteit Rotterdam

Content

Introduction

The regulation of urination is organized in a hierarchical manner within the central nervous system (CNS) and the peripheral nervous system (PNS). This regulation is achieved through coordinated activity between the bladder wall (including the detrusor muscle), the bladder neck, the urethra and the urethral sphincters, which form the lower urinary tract (LUT). In healthy individuals, the control of storing and evacuating urine is managed by specific regions within the spinal cord (such as Onuf's nucleus), the brainstem (including periaqueductal gray [PAG] and Barrington's nucleus [Bar], often referred to as the pontine micturition center [PMC]), as well as higher cortical and subcortical areas (such as the prefrontal cortex [PFC], anterior cingulate cortex [ACC], insula, and thalamus). The primary function of this regulatory network is to initiate urination when a suitable time and place are identified as safe and socially acceptable, and to store urine in the meantime [1, 2]. Problems can occur with the storage or voiding of urine, which can be caused by many diseases and conditions. These problems considering the lower urinary tract are called lower urinary tract symptoms (LUTS). This includes a wide range of symptoms, including voiding/obstructive symptoms (such as prolonged micturition, feeling of incomplete bladder emptying, poor and/or intermittent stream, hesitancy) or storage/irritative symptoms (such as urgency, frequency, nocturia and urge incontinence) [3]. Overactive bladder (OAB) is a syndrome subgroup of storage symptoms characterized by the key symptom: the sensation of urinary urgency. This symptom often goes along with nocturia and frequency, with or without urgency incontinence, without signs of urinary tract infection or other obvious pathology [4]. OAB can occur in individuals without an underlying disease, but it can also be associated with certain neurological conditions, such as Parkinson's disease (PD). PD is a degenerative neurological movement disorder, which is associated with OAB symptoms, most importantly nocturia, urgency, frequency and urinary incontinence [5]. These symptoms are present in 27-86% of PD patients and are suggested to increase in severity with the progression of PD [6].

One crucial component within the brain-bladder pathways is the PAG, and numerous studies have underscored its significance in controlling LUT function. The PAG is situated in the midbrain (Figure 1), and acts as a connection between higher brain centers responsible for decision-making and lower centers involved in micturition. Therefore, it facilitates bidirectional communication between the brain and the bladder. The PAG receives sensory input from the bladder, projects it to various regions of the forebrain, and sends motor signals to the bladder and urethra via the PMC, as portrayed in Figure 2 [7].

Within the brainstem, the PMC is located in the medial dorsal pons (Figure 1) and consists mainly of Bar and is close to, or includes the laterodorsal tegmental nucleus (LDTg) and locus coeruleus (LC). The terms Bar and PMC are often used interchangeably in the literature. However, PMC typically refers to the functional region responsible for coordinating bladder control. This functional region likely involves the neurons from Bar, but may also include other neurons, such as those from the LC and the LDTg [8]. The PMC works with other regions of the brain to coordinate micturition and receives excitatory and inhibitory input from the PAG. Animal studies showed that Bar receives input from the lateral hypothalamic area, preoptic area and the LC [8]. The PMC projects directly to bladder detrusor motor neurons in the sacral spinal cord and indirectly to urethral motor neurons via Onuf's nucleus (Figure 2). Thus, during storage the PAG is activated by afferent input from the bladder and the PMC is inactive. When a certain volume threshold, and therefore a certain amount of distension, in the bladder is reached, the switch from storage to micturition can take place if there is no supratentorial control. This occurs by an excitatory signal send from the PAG to the PMC, which is associated with the PMC activation. The PMC sends descending signal to the sacral spinal nuclei resulting in the initiation of voiding. It is thought that the PMC also receives a 'safe to void' signal from the hypothalamus. Some evidence exists that a third brainstem nucleus is involved in LUT control. This nucleus would be located lateral and ventral to the PMC and is not

directly connected to it. It is called the pontine storage center (PSC), or the L-region. Excitation of this region is thought to promote storage by tightening the external urethral sphincter (EUS) [7, 9, 10].

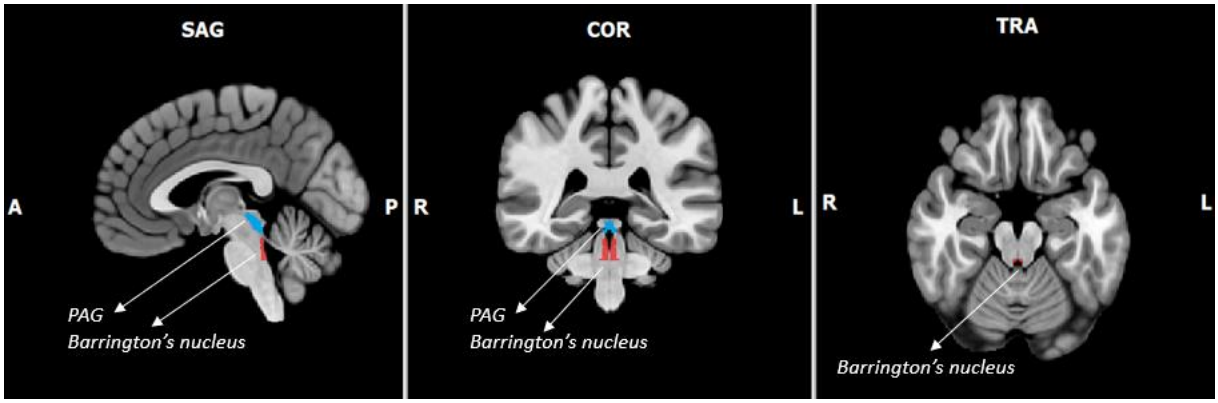

Figure 1: localization of the periaqueductal gray (PAG) and Barrington's nucleus (Bar), often referred to as the pontine micturition center (PMC) in a sagittal, coronal and transversal slice.

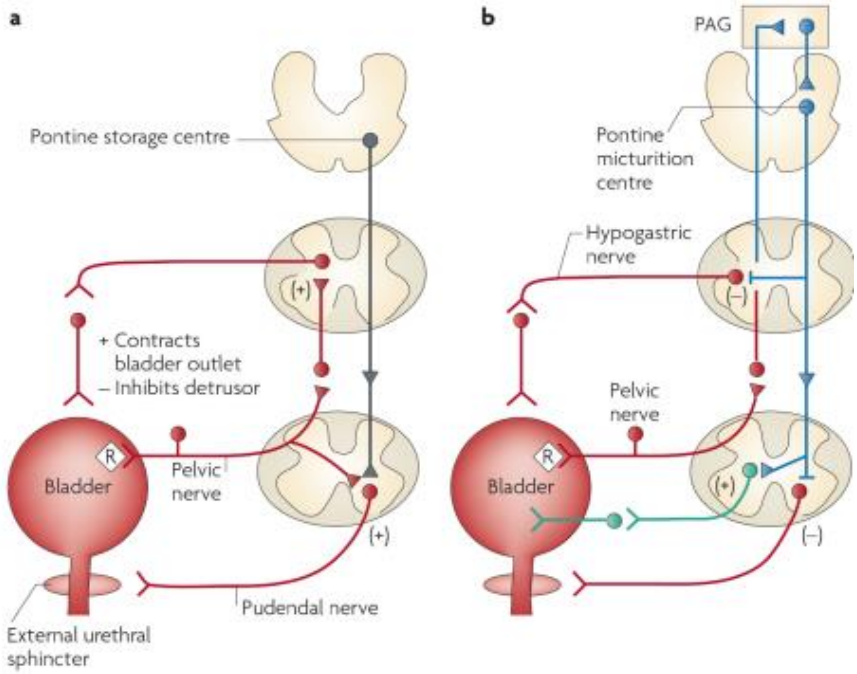

Figure 2: Graphical representation of neural circuits regulating continence and micturition. (a) Reflexes for urine storage. Storage of urine increases bladder distention which produces vesical afferent firing. This activates sympathetic outflow through the hypogastric nerve towards to bladder outlet and the pudendal outflow directed to the external urethral sphincter. These reflexes are mediated by spinal reflex pathways and represent guarding reflexes promoting continence. Simultaneously, sympathetic firing hinders detrusor muscle contraction and modulates neurotransmission in bladder ganglia. Within the rostral pons, a specific region known as the pontine storage center may enhance activity in the striated urethral sphincter. (b) Reflexes for voiding. During voiding, afferent firing from the bladder to the pelvic nerve activates spinobulbospinal reflex pathways (blue) which pass through the pontine micturition center. This activation leads to stimulation of parasympathetic outflow to the bladder and urethral smooth muscle (green), while inhibiting sympathetic and pudendal outflow to the urethral outlet (red). Afferent information from the spinal cord may pass through relay neurons in the periaqueductal gray before reaching the pontine micturition center. These pathways do not represent conscious bladder sensations or mechanisms showing the switch from storage to voiding [7].

In order to investigate interactions between different brain regions involved in micturition, functional Magnetic Resonance Imaging (fMRI) scans are used. fMRI is a valuable tool for measuring brain activity by detecting changes in oxygenated and deoxygenated hemoglobin. Activation in brain regions results in a regional increased cerebral blood flow (CBF), altering the ratio of oxygenated and deoxygenated hemoglobin. These alterations are reflected in blood-oxygen-level-dependent (BOLD) signals, which are captured by the MRI scanner. The BOLD signals reflect the brain activation, allowing fMRI to capture brain activity over time [11-13]. Using fMRI, the interaction between different brain regions can be investigated by measuring the similarity between BOLD signals from two distinct brain regions [12-14]. Most fMRI studies focus on cortical regions, while investigations of brainstem regions are less frequently performed and often encounter unique challenges. The main challenge is the small size of the structures of interest, the brainstem nuclei. These structures are typically only a few millimeters in size, compared to larger cortical structures. This makes it necessary to obtain a higher spatial resolution for brainstem investigations. Improving spatial resolution is accompanied by a drop in signal-to-noise ratio (SNR) [15]. These problems can be overcome by usage of ultra-high field (UHF) MRI scanners, which are scanners with a field strength of 7T or higher. In general, advantages of structural and functional UHF imaging are the increased SNR and contrast-to-noise ratio (CNR). The combination of these effects allows reduction of voxel size compared to 3T MRI without significant signal loss. This allows for sub-millimeter spatial resolution and is therefore essential for the investigation of the functional connectivity in the brainstem [16].

The preprocessing of fMRI data is a critical step in fMRI research, involving a series of procedures to prepare raw imaging data for analysis. It ensures the data accurately reflects brain activity, it reduces noise and variability, and enhances the reliability and comparability of results across subjects [17]. A common preprocessing step includes the normalization of data to Montral Neurological Institute (MNI) space, which is a common coordinate system. Transforming data into this reference space facilitates comparison of the data between datasets [18]. However, an often occurring problem in fMRI research of the brainstem is the suboptimal registration of the structural and functional data to MNI space, since most registration tools focus on cortical regions instead of the brainstem. Since brainstem structures are small and in close proximity to each other, optimal registration to MNI space is crucial [15].

Previous studies of our group used UHF fMRI for the investigation of functional activity in the PAG. Functional activity was investigated in subjects both during an empty bladder state and in a full bladder state during the fMRI scan. Using the acquired data, functional connectivity patterns between the PAG and Bar were investigated. These studies provided insights into different functional parts in the PAG and their distinct functional connectivity patterns with Bar. This demonstrated functional mapping of the brainstem is possible and provided necessary advancements to investigate functional activity and connectivity patterns for subregions of the brainstem using UHF neuroimaging.

One of the most important regions in the brainstem involved in micturition is Bar, which is located in the pons. It is suggested other areas within the pons are involved in micturition pathways as well, such as the PSC, LC or raphe nucleus [7, 9, 19-21]. However, it is unclear what regions within the pons show interaction with Bar. Therefore, this study aims to investigate functional connectivity patterns between Bar and other regions in the pons using 7T fMRI scans . It is expected that regions exist within the pons that show a high correlation with Bar.

In order to investigate this, two datasets are utilized. One dataset contains subjects suffering from PD and healthy subjects, without a specific focus on bladder state. The PD subjects can further be classified based on the presence or absence of LUTS. The other dataset contains subjects during an empty bladder and full bladder state. We hypothesize that specific areas within the pons exhibit a high correlation with Bar. Moreover, these correlations should be consistent across both datasets, thereby enhancing the reliability of the findings. Differences in functional connectivity patterns will be investigated for PD

subjects with or without LUTS, and for subjects during different bladder states. This way it can be investigated whether certain areas within the pons are involved in the manifestation of LUTS in PD patients or are different during certain bladder states. We expect that functional connectivity patterns will differ based on the presence of LUTS in PD patients and will vary based on bladder state. In order to facilitate these analyses, a tool will be developed to improve the registration of structural and functional data to MNI-space, in order to improve the quality of the analysis.

Clinical Background

Lower urinary tract control

Anatomy and physiology:

Micturition is a complex process and its control involves different parts of the central and peripheral nervous system via many pathways and different neurotransmitters. To obtain a better understanding of the working mechanisms, the anatomy and physiology of the storage and voiding of urine will be discussed here.

Peripheral nervous system

Efferent innervation and neurotransmitters

The efferent part of the peripheral nervous system that innervates the lower urinary tract can be divided into three parts: the sympathetic, the parasympathetic and the somatic nervous systems (Figure 3).

The sympathetic nervous system originates from the thoracolumbar region of the spinal cord (T11 – L2). Axons run in the inferior mesenteric ganglia and hypogastric nerves through inferior splanchnic nerves into the pelvic plexus and genitourinary organs. Sympathetic activation inhibits micturition by relaxation of the detrusor muscle and constriction of the urethral sphincter. Sympathetic axons synapse with β2 and β3 receptors in the detrusor wall. Sympathetic activation causes release of noradrenaline which activate the β3- adrenoceptors, leading to relaxation of the detrusor. Moreover, release of noradrenaline leads to response of α1-adrenoceptors of the bladder base and urethra by contraction of the bladder neck and urethra. Both mechanisms contribute to the storage of urine.

The parasympathetic nervous system initiates micturition by contraction of the detrusor while inhibiting the contraction of the external urethral sphincter (EUS). Parasympathetic fibers originate from the sacral spinal cord (S2-S4) of which the neurons are located in the sacral parasympathetic nucleus (SPN). These neurons send axons through the ventral root, through the pelvic nerves and connect with the pelvic plexus before ending on the surface of the bladder, bladder wall and urethra. Activation of this system causes release of acetylcholine (ACh) which activates M2 and M3 receptors in the bladder, causing bladder contraction [7].

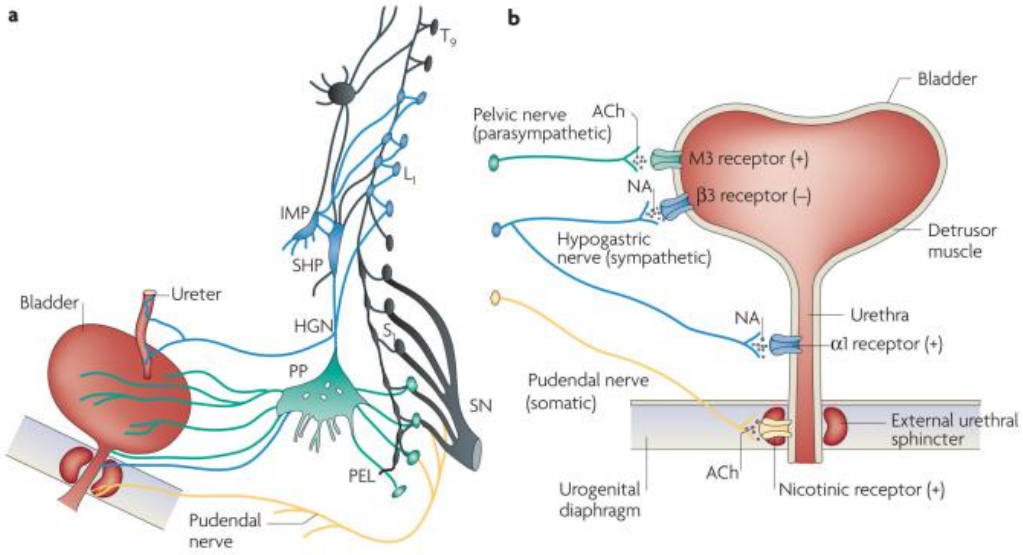

Figure 3: Efferent pathways of the lower urinary tract. (a) Sympathetic fibers (blue) from T11-L2 segments run through the mesenteric ganglia (inferior mesenteric plexus, IMP) and the hypogastric nerve (HGN) or through the paravertebral chain. Eventually, the pelvic nerves at the base of the bladder and urethra are reached. Parasympathetic fibers (green) from S2-S4 spinal segments travel in sacral roots and pelvic nerves (PEL), via the pelvic plexus (PP) to the bladder wall. Somatic motor neurons (yellow) supply the striated muscles of the external urethral sphincter (EUS). These fibers arise from S2-S4 motor neurons and pass through pudendal nerves. (b) Efferent pathways and neurotransmitter mechanisms regulating the lower urinary tract are displayed. Parasympathetic postganglionic axons in the pelvic nerve release acetylcholine (ACh), inducing bladder contractions by stimulating M3 muscarinic receptors in the bladder smooth muscle. Sympathetic postganglionic neurons release noradrenaline (NA), activating β3 adrenergic receptors to relax bladder smooth muscle and α1 adrenergic receptors to contract urethral smooth muscle. Somatic axons in the pudendal nerve also release ACh, causing contraction of the external sphincter striated muscle by activating nicotinic cholinergic receptors [7].

The somatic pathways originate from the sacrum (S2-S4) at Onuf's nucleus and run through the pudendal nerve to the EUS. In the EUS, nicotinic receptors are present, and when stimulated by acetylcholine released from the somatic nerves (specifically the pudendal nerve), the sphincter will contract. The control of the EUS is under semi-voluntary control, allowing for conscious regulation of micturition, and involves a complex interaction between somatic, sympathetic, and parasympathetic systems, including the release of NO in the sphincter [22]. The pudendal nerve, together with the hypogastric nerve, provides sensory information from the bladder neck and urethra to the central nervous system [7].

Afferent innervation:

Sensory information from the lower urinary tract is transmitted via the axons of afferent neurons of the pelvic, hypogastric, and pudendal nerves. The pelvic and hypogastric nerves provide information about bladder fullness, whereas the pudendal and hypogastric nerves carry sensory information from the bladder neck and urethra.

The afferent components of these nerves consist of myelinated (Aδ) and unmyelinated (C) axons. Aδ-fibers are sensitive to passive distension and active contraction, providing information about bladder filling. Specifically, Aδ-nerve fibers in the detrusor muscle respond to bladder distension and contraction, relaying information about bladder filling. The critical activation values for Aδ-fibers range from 5–15 mmH2O, corresponding to the pressures at which humans perceive bladder filling. In contrast, C-fibers

are typically insensitive to physiological bladder filling (hence they are called 'silent' C-fibers), responding primarily to noxious stimuli such as chemical irritation or cooling. Both Aδ-fibers and C-fibers originate from cell bodies in the dorsal root ganglia (DRG) at the S2–S4 and T11–L2 spinal segments. These axons connect with interneurons participating in spinal reflexes and spinal-tract neurons projecting to higher brain centers involved in bladder control [23].

Central nervous system

The regulation of micturition involves connections between different brain regions and tracts in the spinal cord (including sympathetic, parasympathetic and somatic systems). Sympathetic and parasympathetic preganglionic neurons are located lumbosacral in the intermediate Gray matter (laminae V-VII). The somatic motor neurons which innervate the EUS lie in Onuf's nucleus (lamina IX). The brainstem, which includes the midbrain, pons, and medulla oblongata, is located in the lowest part of the brain. Among these components, the pons contains the PMC, a secondary control center that sends signals to stop bladder relaxation and start relaxation of the external sphincter when it's time for micturition. The cerebrum is able to inhibit the micturition reflex. The PAG is a key part of the brain that occupies an important position between the cerebrum and bladder, acting as a switchboard between brain and bladder in order to make decisions regarding urination. Under normal conditions, the switch between storage and voiding of urine is managed by the spinobulbospinal reflex. During the storage of urine, when the bladder fills, afferent signaling get stronger until a certain limit in the brainstem (specifically the PAG) is reached. In absence of supratentorial control, reflex micturition is triggered. The PMC will be activated and micturition starts due to sphincter relaxation and bladder contraction. The PAG may also interact with other brain regions, potentially influencing the emotional aspects of urination, such as determining whether it is safe, emotionally and socially appropriate to urinate. Brain imaging research has identified mechanisms in the cerebrum for regulating micturition. The cerebrum inhibits bladder contractions and processes afferent signals from the bladder and urethra, leading to the sensation of the urge to void. The micturition reflex remains suppressed until a decision to void is made in the prefrontal lobe in the prefrontal cortex or limbic system. These circuits will be discussed beneath (see Figure 4) [7, 23, 24].

Control of the lower urinary tract function is built like an on-and-off mechanism. When the bladder is filling, storage mechanisms are activated which are mainly peripheral mechanisms (see 'Regulation of urine storage'). Meanwhile the mechanisms involving voiding are mainly central mechanisms (see 'Regulation of micturition), Figure 4.

Regulation of urine storage

Several reflexes contribute to the maintenance of urine storage. One of these reflexes is called the sympathetic reflex. This reflex is evoked by a sarco-lumbar intersegmental spinal reflex pathway and is activated by vesical afferent activity in the pelvic nerves. When bladder pressure reaches a certain threshold, the reflex pathway is inhibited. Thus, it acts as a negative feedback mechanism, allowing the bladder to contain larger volumes during filling but turning off during micturition.

Other reflexes involved in storage mechanisms are guarding reflexes. The EUS, innervated by motoneurons, exhibits a tonic discharge that increases during bladder filling. Contraction of the sphincter sends afferent information through the pudendal nerves, activating interneurons in the spinal cord. This mechanism suppresses bladder activity by inhibiting parasympathetic preganglionic neurons, thereby inhibiting the micturition reflex pathway. Activation of the pudendal nerve initiates reflex contractions of the EUS, further contributing to continence. Another guarding reflex serves as a defense mechanism against accidental urine leakage resulting from sudden or involuntary rises in bladder pressure, commonly known as stress incontinence. In case sudden bladder pressure elevations occur (such as during coughing, sneezing, standing, or laughter), afferent nerve fibers transmit signals to Onuf's nucleus, which activates efferent fibers, causing the EUS to contract [9].

Studies involving cats have found that electrical stimulation of the area ventrolateral to the PMC and located in the pontine tegmentum, known as the PSC or L-region, serves a multifaceted role. Besides exciting the EUS, the reflex bladder activity is inhibited, thereby increasing bladder capacity while attenuating the bladder's excitatory response to PMC stimulation. Neurons within the PSC region project to the nucleus raphe magnus (NRM) in the medulla. This region contains neurons that project to the lumbosacral spinal cord. Stimulation of the NRM, either electrically or chemically, triggers serotonergic inhibition of reflex bladder activity [9, 25-27]. Consequently, the neurons within the PSC may initiate descending inhibitory pathways to the sacral parasympathetic nucleus [9, 28]. Moreover, the PSC projects to the motor neurons of the urethral sphincter in Onuf's nucleus. Stimulation of the PSC seems to excite the pelvic floor musculature, increase the urethral pressure and increase urethral contraction [29-32]. In one study, urethral contraction with possible detrusor inhibition and mixed sphincter response combinations were found when stimulating an area which included the L-region, but was not limited to this area only. Next to this, bilateral ablation of the L-region caused severe detrusor overactivity and incontinence [30, 32]. These results are found in studies involving cats, however it is relatively unclear whether the same mechanisms exist in humans. PET-scans in humans provided evidence for a possible PSC in humans. Subjects were asked to void inside the scan, and in subjects who could void activation in the PMC was registered. Subjects who were unable to void, no activation of the PMC was found, but activation ventrolateral of the PMC was seen, at the predicted location of the PSC in cats. The subjects that were unable to void contracted their urethral sphincter and could not void, although their bladder was full and they tried to void [29, 33, 34].

Regulation of micturition

The switch from the storage phase to the micturition phase can occur involuntarily (reflexively) or voluntarily. In normal adults this switch is under voluntary control, and are therefore able to postpone or hasten the moment of urination so it occurs when it is emotionally safe, socially appropriate and consciously desired. Without supratentorial control, reflex micturition is triggered when the level of urine exceeds a certain sensory limit for voiding. The PAG will send excitatory signals to the PMC, which results in inhibition of sympathetic and somatic nerves and activation of parasympathetic pathways. This causes the bladder to contract, increasing intravesical pressure and the flow of urine. The EUS relaxes due to release of nitric oxide (NO) by parasympathetic nerves and the elimination of adrenergic and somatic cholinergic excitation. Moreover, secondary reflexes which are generated by the flow of urine facilitate emptying of the bladder [7, 23].

Functional imaging studies have shown that different brain regions are involved in micturition, including the prefrontal cortex, the insula, the hypothalamus, the PAG, and the PMC. Some of the involved neural circuits in the forebrain and brainstem will be discussed next and are shown schematically in Figure 4:

Circuit 1: prefrontal cortex and insula

An important circuit includes the thalamus, insula, lateral prefrontal cortex (lPFC), medial prefrontal cortex (mPFC) and the PAG. The insula has a homeostatic afferent role and registers visceral sensations. It receives afferent homeostatic information from the spinal cord, relayed in the thalamus, such as the sensation of bladder filling. Insular activation increases with bladder filling. This sensation, for example, is absent in women with impaired bladder sensation (Fowler's syndrome) [9, 35]. The prefrontal cortex also plays a role in bladder control. It is located anteriorly to the motor strip, and ventromedial areas are involved in decision-making in a social and emotional context. The circuit is closely connected with the limbic system (including the hypothalamus and amygdala), the anterior cingulate cortex (ACC), and the insula. The more laterally located parts of the prefrontal cortex are more involved in cognitive functions such as the working memory, and its activation has been shown in several bladder studies [9, 34, 36].

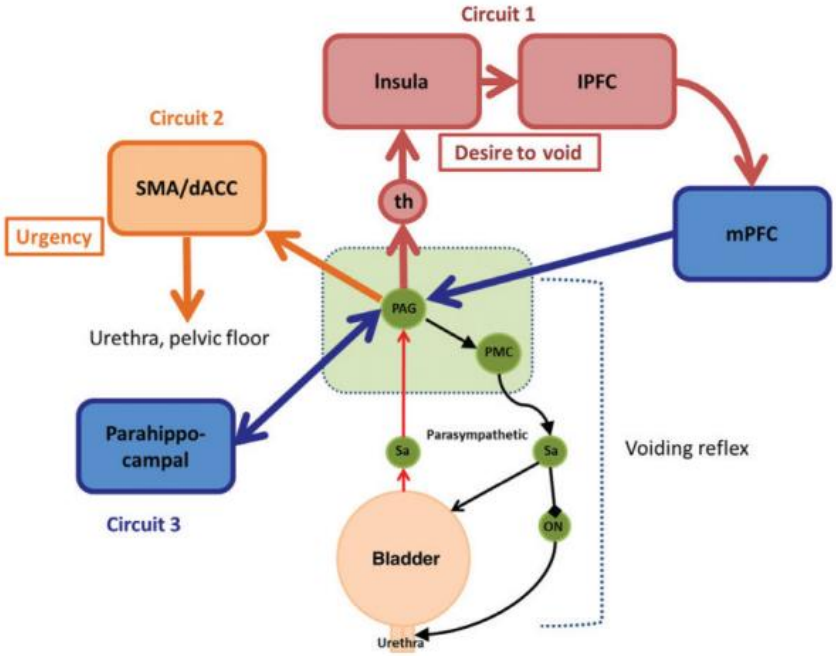

Figure 4: Simple working model of lower urinary tract system, showing the voiding reflex, brainstem (green) and circuits 1, 2, and 3 (red/blue, yellow and blue). PAG = periaqueductal gray, PMC = pontine micturition center, th = thalamus, mPFC = medial prefrontal cortex, lPFC = lateral prefrontal cortex, SMA = supplementary motor area, dACC = dorsal anterior cingulate cortex, Sa = sacral parasympathetic region, ON = Onuf's Nucleus [9].

Circuit 2: dorsal anterior cingulate cortex (dACC) and supplementary motor area (SMA)

Interoceptive sensations are characterized by their connection to an affective and motivational dimension, playing a role in maintaining homeostasis. For instance, the escalating discomfort to void resulting from bladder filling ensures regular emptying. The exact timing and location, however, of bladder emptying remain under voluntary control. The ACC can be seen as the limbic motor cortex, which means it modulates and motivates bodily arousal states. Activation of the ACC could activate the sympathetic nervous system, causing inhibition of micturition. The dACC is usually coactivated with the SMA, and these activations are associated with contraction of the pelvic floor muscles and muscles of the sphincter [9, 37]. Pelvic floor muscle contractions seem to provoke stronger sensations and greater SMA responses when the bladder is full, compared to when it is empty. As schematically shown in Figure 4, pathways are not clearly connected in Circuit 2. Probably, the efferent signal from the PAG to the dACC/SMA is transferred via the thalamus [9, 38].

In case of urge urinary incontinence, the dACC and SMA seem capable of generating both the sensation of urgency and contraction of the urethral sphincter. This dual response facilitates a prompt toilet visit while reinforcing the ability to postpone voiding until reaching the toilet. This circuit is most likely a back-up continence system in patients with urgency incontinence or OAB complaints when they experience urgency [9].

Circuit 3: subcortical mechanisms

In individuals without underlying conditions, the bladder typically undergoes gradual filling, often without conscious sensations, but likely involving subconscious brain monitoring. During this early stage of bladder filling, when the bladder volume is small and sensations are minimal, a subcortical network is activated, involving the PAG and segments of the inferior or middle temporal (parahippocampal) cortex. Simultaneously, cortical regions do not seem to play a role then, reflecting the absence of bladder filling sensations [9].

In the case of women with Fowler's syndrome, characterized by a lack of bladder sensations and difficulties in bladder emptying, the restoration of bladder sensations through sacral neuromodulation induces changes in similar networks in the brainstem/parahippocampal network. They found activation again, especially the midbrain, in the Fowler's syndrome patients after sacral neuromodulation [39]. This suggests that this network might be the pathway through which the PAG typically monitors the bladder state and communicates these signals from the bladder to other brain regions. Given the close location of the parahippocampal cortex to the amygdala (the center of emotional processing), the circuit is likely to be concerned with the emotional aspects in voiding, such as feelings of "safety". It may potentially transport signals to brainstem nuclei via the hypothesized "safe" signal from the hypothalamus [9].

Parkinson's Disease and LUTS

PD is a degenerative, progressive neurologic movement disorder which results in motor symptoms such as resting tremor, bradykinesia, (cogwheel) rigidity, and postural instability. PD affects approximately 100 to 180 individuals per 100,000 in the population, with an annual incidence rate of 4 to 20 per 100,000 people. PD is characterized by the degeneration of dopamine producing cells in the substantia nigra of the midbrain and by Lewy body formation. It has been proposed that the intraneuronal Lewy body formation and Lewy neuritis begin at two anatomical locations and continue in six stages. During this process, components of other systems become gradually involved. In the first two stages, the Lewy body formation is restricted to the medulla oblongata / pontine tegmentum and anterior olfactory structures. In stage 3 to 4 the substantia nigra, other nuclei of the basal mid- and forebrain, and the mesocortex become affected. The clinical manifestation emerges during these stages. At last, during stage 5 and 6, lesions will appear in the neocortex. Next to the motor symptoms, nonmotor symptoms also emerge, which could significantly negatively influence the quality of life of individuals. These symptoms include constipation (>50%), dysphagia (30%–82%), depression (>16%), orthostatic hypotension (20%–58%), cognitive decline and dementia (>6 times higher compared to healthy individuals), sexual dysfunction (43%–81%), and LUTS [6].

The prevalence of LUTS in PD patients has a wide range of approximately 38% – 71%, which is significantly more compared to healthy controls. LUTS are usually classified as storage or voiding symptoms [3]. Storage symptoms could indicate detrusor hyperreflexia, wherein bladder contractions occur at urinary volumes that normally would not trigger bladder activity. Voiding symptoms can arise from bladder hypoactivity or an obstruction in the lower urinary tract. Storage symptoms predominate in Parkinson's disease. Nocturia is the most common occurring symptom, affecting 57% - 86% of PD patients, followed by frequency (32% - 71%), urgency (32% - 68%), and urge incontinence (21% - 40%). Hesitancy occurs in 1% - 38% of PD patients and incomplete emptying occurs in 8% - 28% of PD patients.

There are indications that the severity of LUTS in PD patients correlates with the stage of the disease. Moreover, it is suggested both motor and nonmotor symptoms could affect the severity of LUTS. Tremor, impaired mobility, gait, balance deficits along with challenges in maintaining attention, are thought to worsen urinary urgency and other bladder symptoms [6, 40].

In PD, dopamine producing cells in the substantia nigra of the midbrain degenerate, causing cell depletion in the substantia nigra pars compacta. Dopaminergic mechanisms influence micturition through D1 and D2 receptors located in the striatum, exerting both inhibitory and excitatory effects, respectively. Dopaminergic neurons are predominantly located in the substantia nigra pars compacta and the ventral tegmental area of the midbrain. Neural firing in the substantia nigra and the release of striatal dopamine activate the dopamine D1-GABAergic direct pathway via D1 receptor activation in the striatum. This pathway inhibits basal ganglia output nuclei, as well as the micturition reflex through GABAergic collaterals to the micturition circuit, particularly to the PAG (Figure 5). Consequently, the degradation of the substantia nigra leads to a decrease in D1-mediated inhibition, potentially resulting in detrusor overactivity and urgency/frequency complaints. Additionally, in the indirect pathway, it was found that high frequency stimulation of the D2 receptors, (leading to inhibition) inhibits the subthalamic nuclei (STN) which results in bladder inhibition. Therefore, the micturition reflex seems to be influenced by dopamine in an inhibitory (via D1) and facilitatory (via D2) way [6, 20, 40, 41].

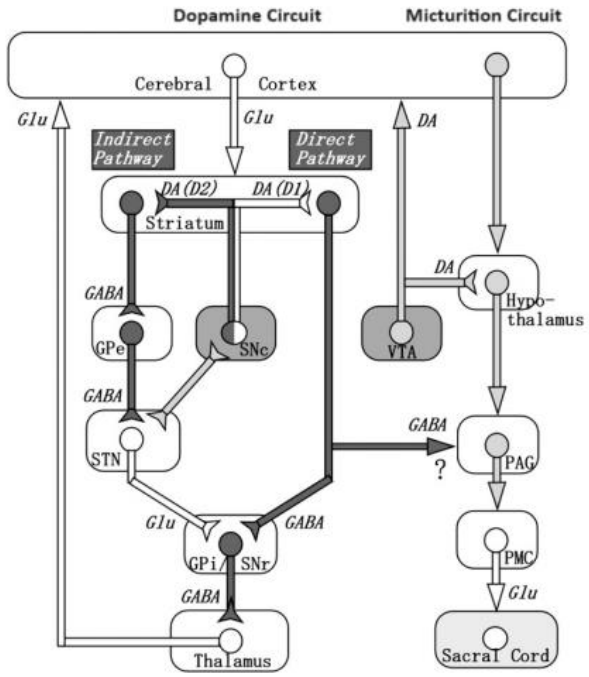

Figure 5: Probable relationship between dopamine circuit (left) and micturition circuit (right). The micturition reflex is influenced by dopamine (DA), as well as by inhibitory (D1) and facilitatory (D2) and gamma-aminobutyric acid (GABA, inhibitory). Neural firing of the substantia nigra pars compacta (SNc) and the released striatal dopamine activates the dopamine D1-GABAergic direct pathway. This inhibits the basal ganglia output nuclei (GPi, SNr) and inhibits the micturition reflex via GABAergic collateral to the micturition circuit. High frequency stimulation (inhibitory signal) in the STN also leads to bladder inhibition.

Key terms: DA (dopamine), GABA (gamma-aminobutyric acid), SNc (substantia nigra pars compacta), GPi (globus pallidus internus), SNr (substantia nigra pars reticulata), STN (subthalamic nucleus), GPe (globus pallidus externus), VTA (ventral tegmental area), PMC (pontine micturition center), Glu (glutamate). White lines represent excitatory neurons, black lines represent inhibitory neurons. Hatched lines represent neurons of undetermined property [41].

Technical Background

Basis of Magnetic Resonance Imaging

Magnetic Resonance Imaging (MRI) is an imaging technique which makes use of magnetic fields and radio magnetic waves to enable detailed visualization of both functional and anatomical data of the human body, including the brain. The basis of MRI lies in the nuclear magnetic resonance principles. During MRI, body tissues are magnetically excited, and the returned electromagnetic signals from the body are recorded. Nuclei with an odd number of protons or neutrons are magnetically excitable, with the hydrogen isotope ^{1}H commonly used in medical MRI scans due to its abundance in the human body and its favorable magnetic properties. Protons possess magnetic properties due to their intrinsic spin and magnetic moment. In an MRI scanner, the patient is placed in a strong magnetic field, which makes it possible to align these protons to this magnetic field. This external field is called the B_0 field. In addition to spinning around their own axis, protons spin (precess) around the axis of the B0 field. A radiofrequency (RF) pulse is then transmitted into the body within the magnetic field, disrupting the equilibrium state of the protons. This causes the protons to flip 90 degrees relative to the B_0 field and to precess in phase during the RF pulse. When the RF pulse is turned off, the protons begin to reorient along the B0 field and dephase (spin out of phase). T1 (longitudinal relaxation time) is the time constant that determines the rate at which excited protons return to equilibrium, aligning along the B_0 field. T2 (transverse relaxation time) is the time constant which determines the rate at which excited protons go out of phase with each other. The speed of this decay depends on the physiological properties of the tissue and local field inhomogeneities, such as the state of the local blood oxygenation. Due to these magnetic field inhomogeneities in the B_0 field and physiological tissue, the spins of the protons dephase faster than T2-time rate, referred as the T2*. The fact that these local field inhomogeneities lead to different precession frequencies (increasing the dephasing speed) is an important observation for (f)MRI. The local field inhomogeneities are dependent on the local physiological state, mostly the state of local blood oxygenation, which is dependent on the state of local neuronal activity (in the brain). All these signals are eventually used to reconstruct images of the structures of the body, such as the brain [11].

Functional MRI (fMRI) and the BOLD Response

Functional MRI (fMRI) is based on the techniques of MRI by mapping both the functional activity of the brain and its anatomy. fMRI utilizes the BOLD response to measure changes in brain activity. The BOLD response is dependent on differences in the magnetic properties of oxygenated and deoxygenated hemoglobin. Neuronal activity consumes energy, which requires glucose and oxygen supplied by the vascular system. Thus, neuronal activity leads to an increase in local blood flow which, combined with an oversupply of oxygenated blood, results in an increased concentration of oxygenated blood in active regions. Hemoglobin, which carries oxygen in red blood cells, exhibits different magnetic properties depending on its oxygenation state. Deoxygenated hemoglobin is paramagnetic, which distorts the magnetic field, leading to faster dephasing of protons and therefore weakening the MRI signal. Oxygenated hemoglobin is diamagnetic, which has a less disruptive effect on the magnetic field, resulting in a stronger MRI signal (Figure 6). Consequently, differences in brain activity lead to changes in the ratio of oxygenated to deoxygenated hemoglobin, which in turn leads to variations in the MRI signal. These differences in signal intensity lie at the basis of fMRI and through statistical analyses can be used to create maps of brain activity related to specific tasks of stimuli. Thus, fMRI provides an indirect measurement of neural activity by assessing changes in blood oxygenation at a given time, resulting in BOLD signals [11]. The similarity of these BOLD signals between two different brain regions during a specific task or state, could indicate that these regions interact with each other, commonly referred to as functional connectivity [14]. fMRI is therefore often used in neuroscience to investigate functional organization of the brain and map brain networks [11].

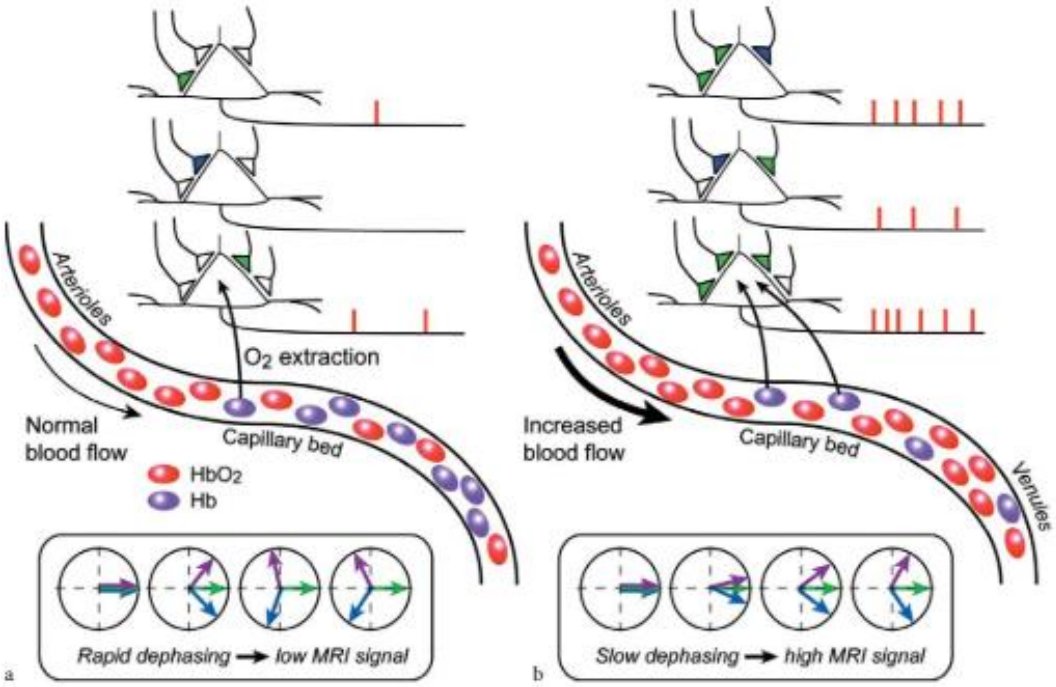

Figure 6: BOLD responses are used in fMRI. (a) Baseline neural activity is represented and basal cerebral blood flow (CBF) takes place. A constant oxygenated blood flow due to a constant neural activity, leads to a fixed oxygenated to deoxygenated hemoglobin ratio. Since hemoglobin is paramagnetic, it disrupts the magnetic field, leading to relatively rapid dephasing and a lower MRI signal. (b) In case the neural activity increases, the oxygenated blood supply will increase in this region. Since oxygenated hemoglobin is diamagnetic, and therefore has a less disruptive effect on the magnetic field, the relative dephasing becomes slower which leads to a higher MRI signal [11].

Methods

In this research, two datasets were used. The first dataset contains fMRI scans of subjects based on bladder sensations and bladder state, and will be referred to as the fMRI bladder state study. The second dataset contains fMRI scans of a population consisting of patients with PD and healthy controls, without registration or emphasis on bladder sensations or bladder state. This study will be referred to by TRACK-PD study.

Participants

The first dataset contains a total of seven subjects: five healthy female participants without a history of LUT dysfunction, neurological disorders or other dysfunction, and two subjects with OAB. In this research, only female participants were chosen in order to control for gender as a confounding factor. The inclusion and exclusion criteria for the healthy controls and the OAB patients are shown in Table 1. In Table 2 the patients characteristics of the fMRI bladder state study are shown.

In the TRACK-PD study, 106 PD patients and 45 healthy controls were included. The PD patients were recruited from the movement disorder clinic of the Department of Neurology at Maastricht University Medical Centre + (MUMC+) and other collaborating hospitals. The healthy controls were recruited through social media, websites and via patient meetings [42].

In order to participate in the study, the following inclusion criteria were applied: 1) PD patients must have been diagnosed by a neurologist within the three years prior to inclusion; 2) A Montreal Cognitive Assessment (MoCA) of ≥24 must be achieved at baseline; 3) Subjects must be able to understand and read Dutch; 4) Age must be 18 years or older; 5) Written informed consent must be obtained. Exclusion criteria included: 1) Advanced cognitive impairment (defined as a score MoCa score < 24, or a dementia diagnosis according to the fifth edition of the Diagnostic and Statistical Manual of Mental Disorders (DSM 5); 2) Another neurodegenerative disease, besides PD; 3) Subjects with a contra-indication for a 7T MRI scan, such as permanent makeup, incompatible metallic devices, and claustrophobia. These exclusion criteria also applied to the healthy control group [42].

Due to technical issues during the preprocessing stage, a portion of the data was not compatible with the analysis proposed for this study. Eventually, a total of 48 subjects were included in the post-processing step, comprising 31 PD patients and 17 healthy controls. In Table 3 the patient characteristics of the TRACK-PD study are shown.

Study procedure

In the fMRI bladder state study, the participants completed two visits: a screening visit and scanning visit. During the screening, informed consent was obtained, and participants were assessed for MRI compatibility as well as the inclusion and exclusion criteria. If they met the inclusion criteria, participants were enrolled in the study. Next, they were asked to fill in a three-day micturition dairy and two questionnaires. The micturition diaries helped participants to assess their bladder fullness on a visual analog scale (VAS) and their perception of urgency on the four-point Indevus Urgency Severity Scale (IUSS) [43]. The questionnaires involved the Hospital Anxiety and Depression Scale (HADS) and the Overactive Bladder questionnaire (OAB-q).

The second visit involved the scanning of the participants. The participants visited the outpatient clinic (MUMC+, the Netherlands) and received a transurethral filling catheter after voiding. The participants were then transferred to the Ultra-High-Field MRI center (Scannexus) and asked to place themselves on the MRI bed in supine position. An MRI-compatible syringe pump was connected to the catheter and a 32-

channel head TxRx coil (NOVA Medical) was used for the scanning protocol. After the scanning protocol finished, the catheter was removed and participants could void in private.

The TRACK-PD study is a longitudinal observational study in which participants will be tracked for 4 years. For this research, only the baseline scans are included, of which the data is collected at MUMC+. A 7T brain fMRI scan was performed and basic clinical and demographic information, such as sex, age, handedness, disease duration, and the total levodopa equivalent daily dose (LEDD) were collected. Additionally, motor, cognitive, neuropsychiatric and autonomic symptoms were assessed using validated questionnaires and rating scales. The assessment of autonomic symptoms was conducted using the Autonomic dysfunction (SCOPA-AUT) questionnaire, which is a reliable and valid tool for evaluating autonomic dysfunction in PD. This questionnaire comprises 25 items related to various autonomic symptoms, including LUTS [42]. Motor functions were evaluated using the unified Parkinson's Disease rating scale (MDS-UPDRS). This scale consists of four parts, assessing the motor and non-motor disabilities in PD. This scale also includes a question about urinary problems and the extent someone suffers from these problems [44].

MRI acquisition

In the fMRI bladder state study, participants were scanned at Scannexus on a 7T MRI scanner (MAGNETOM, Siemens, Erlangen, Germany). The scanning protocol consisted of four scans (Figure 7), lasting approximately two hours in total. The region of interest (ROI) was the supramedullary portion of the brainstem, which included the pons and the PAG.

The first scan was a resting-state empty bladder scan, which included 40 slices. The scan consisted of 420 T2*-weighted multiband echo planar imaging volumes (mb-EPI sequence, acceleration factor = 2, MBfactor = 2, TR = 1400 ms, TE= 22ms, resolution = 1.1x1.1x1.1mm).

Then, the anatomical scan was obtained, involving a T1-weighted whole-brain anatomical scan using a Magnetization Prepared Rapid Gradient Echo sequence with a 0.7x0.7x0.7 mm resolution. This scan was used to overlap with the functional data of the other scans.

The second functional scan was the filling bladder scan (mb-EPI sequence, acceleration factor= 2, MB-factor = 2, TR = 1700ms, TE = 22ms, resolution = 0.9x0.9x0.9mm). During this scan, the bladder was automatically filled with a saline solution at body temperature with a rate of 30ml/min. Meanwhile, the participants had to indicate their bladder fullness (VAS) and urgency (IUSS) with a MRI compatible joystick (Figure 7). This way, bladder sensations could be assessed real-time.

The third functional scan was the full bladder scan. Once participants indicated a level of urgency reaching 2 on the 4-point IUSS scale, the syringe pump and bladder filling protocol were terminated, and a resting-state scan with a full bladder was commenced. This was a rs-fMRI with 420 T2*-weighted multiband echo planar volumes and 40 slices of the ROI (md-EPI sequence, acceleration factor = 2, MB-factor = 2, TR = 1400 ms, TE= 22ms, resolution = 1.1x1.1x1.1mm).

In the TRACK-PD study, the participants were scanned on a 7T MRI scanner (Magnetom, Siemens, Erlangen, Germany), which was equipped with a Nova Medical 32-channel head coil. To reduce the possibility of motion artefacts due to tremor and to reflect clinical practice, the scans were performed on patients during the ON-medication state. Additionally, to reduce movements, participants were asked to watch a movie during the scan. Physiological signals (such as cardiac and respiratory signals) were measured synchronized with the scan start. For optimal planning, a localizer sequence was acquired, and B0 and B1 mapping and shimming were performed to correct for field inhomogeneities.

The scanning protocol consisted of:

1. A whole-brain Magnetization Prepared 2 Rapid Acquisition Gradient Echoes (MP2RAGE) scan, with an acquisition time of 10:57 minutes. This produced a T1-weighted image and a quantitative T1 map. The MP2RAGE scan was paired with a Saturation Prepared with 2 Rapid Gradient Echoes (SA2RAGE) scan, which lasted 2:40 minutes, to eliminate B1-related biases that could affect measurement accuracy.
2. A multi-echo GRE scan, covering 4.8 cm, with an acquisition time of 7:42 minutes. This provided susceptibility (T2*)-weighted images and T2* maps. Quantitative susceptibility maps could also be reconstructed from this scan, which is sensitive to variations in iron concentration.
3. A magnetization transfer-weighted TFL (MTW TFL) scan, covering 3 cm, with an acquisition time of 4:38 minutes. This scan could visualize myelination or nuclei containing neuromelanin, such as the substantia nigra and locus coeruleus.
4. A whole-brain diffusion-weighted scan along 66 random directions, with an average b-value of 2000 s/mm^2, mixed with six B0 volumes and one additional B0 volume, and five diffusion-weighted volumes recorded with the opposite phase-encoding direction. The acquisition time was 9:48 minutes.
5. A whole-brain resting-state fMRI scan with 280 volumes and an additional five volumes recorded with reverse phase-encoding direction. The acquisition time for the resting-state fMRI was 11:12 minutes. During this scan, participants were instructed to focus on a crosshair projected on a screen while letting their minds wander without thinking about anything in particular.

In total, the scan protocol takes just under 60 minutes. Further details can be found in Table 4 [42]. For this research, only the first and last scans were used.

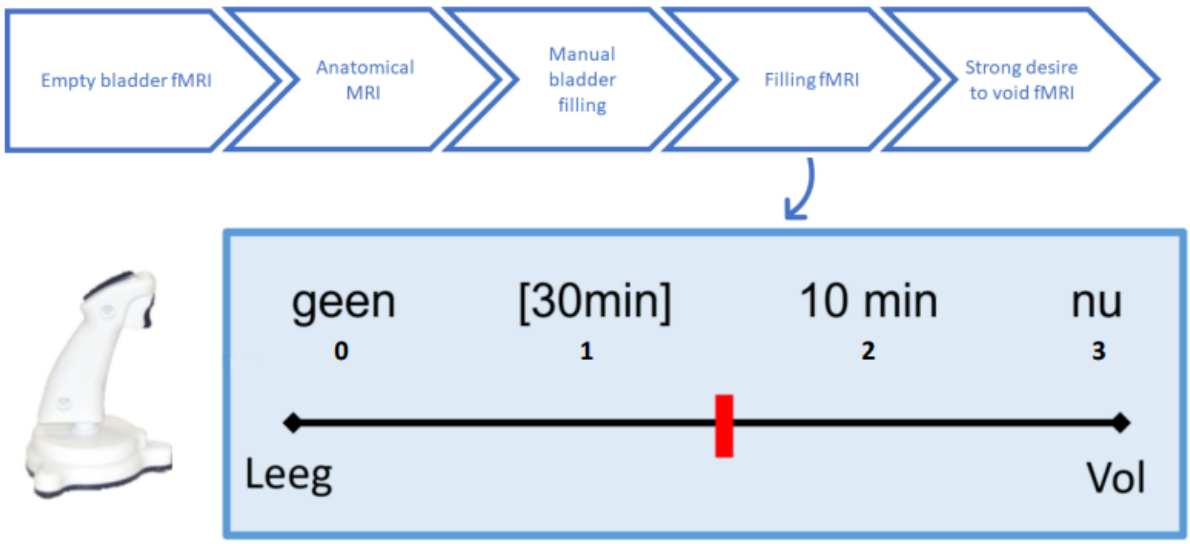

Figure 7: The scanning protocol (above) the IUSS and VAS score (below). In the first row, the scanning protocol of the fMRI bladder state study is shown. This protocol includes an empty bladder fMRI, an anatomical MRI, a filling fMRI and a full bladder fMRI scan. The last row displays the figure participants see during the filling scan, where they indicate their bladd er sensations. The top line represents the IUSS scale, and the bottom part shows the VAS score.

Table 1:

	Inclusion criteria	Exclusion criteria
Healthy subjects	- Healthy female subject - ≥ 18 years old - Written informed consent provided	- History of LUTS symptoms (this exclusion criteria only applies for healthy subjects) - History stress urinary incontinence - History of bladder outlet obstruction - History of urinary tract surgery ≤ 6 months - Indwelling catheter or permanent catheter fitted - Urinary tract infection - Uncontrolled diabetes mellitus - History of fibromyalgia - Pregnant - Pregnancy within 6 months or breast feeding within 3 months before screening - Positive hepatitis A,B, C or HIV - Drug abuse within 3 months prior to the screening visit - History of smoking > 10 cigarette - History of drinking more than 14 units of alcohol per week within 3 months prior to screening - Changes in prescribed medication ≤ 1 month prior to screening - history of treatment with alpha blockers, beta receptor blockers or agonists, botulinum toxin (less than 12 months), resiniferatoxin or pelvic floor muscle relaxants ≤ 9 months prior to screening - clinically significant abnormality during physical examination - Abnormal pulse and/or blood pressure measurements - Participation in any clinical study within 3 months or participation in more than 3 clinical studies within 12 months - Any clinical condition, which, in the opinion of the investigator would not allow safe completion of the study. - Employees of the University of Maastricht involved in the study - MRI contraindications
OAB patients	- Female ≥ 18 years old - Written informed consent provided - History of signs and symptoms of OAB (frequency, urgency or urge incontinence) ≥ 3 months - Naïve to OAB treatment of willing undergo a 3 week washout period	

Inclusion and exclusion criteria of the fMRI bladder state study

Table 2:

fMRI Bladder State Study	Subjects
N	7
OAB patients	2
Healthy controls	5
Gender (F)	7
Mean age	39,3

Patient characteristics of the fMRI bladder state study

Table 3:

TRACK-PD Study	Healthy Controls	PD patients
N	17	31
Gender (F)	5	13
Mean age	60,5	61,5

Patient characteristics of the TRACK-PD study

Table 4:

Weighting	Sequence	TE (ms)	TR (ms)	TI (ms)	Flip angle (°)	FoV (mm)	Resolution (mm^3) (x-y-z)	Slices	Orientation
T1	MP2RAGE	2.51	5000	900, 2750	5 and 3	208	0.65 × 0.65 × 0.65	240	Sagittal
	SA2RAGE	0.78	2400	58, 1800	4 and 10	256	2.0 × 2.0 × 2.0	88	Sagittal
T2*	GRE	2.49, 6.75, 13.50, 20.75	33	–	12	204	0.5 × 0.5 × 0.5	96	Axial
Neuromelanin	MTW TFL	4.08	538	–	8	192	0.4 × 0.4 × 0.5	60	Axial
Diffusion	EPI	60.6	7000	–	90	192	1.5 × 1.5 × 1.5	80	Axial
fMRI	BOLD	18.6	2000	–	70	200	1.25 × 1.25 × 1.25	92	Axial

TRACK-PD study MRI protocol with technical details

Magnetization Prepared 2 Rapid Acquisition Gradient Echoes (MP2RAGE); Saturation Prepared with 2 Rapid Gradient Echoes (SA2RAGE); Gradient Echo (GRE); Magnetization transfer weighted TFL (MTW TFL); Echo Planar Imaging (EPI); Blood oxygen level dependent (BOLD); Echo time (TE); Repetition time (TR); Inversion Time (TI); Field of view (FOV)

Preprocessing

Preprocessing of fMRI data is essential for optimal analysis of the data. These steps convert the data into interpretable brain images, reduce different types of unwanted noise and precondition the data for final statistical analysis [17]. The data from both datasets were preprocessed in the same way using BrainVoyager 22.2 and 23.2 (Brain Innovation, Maastricht, Netherlands) and custom-made Python scripts. These scripts facilitated the automation of specific commands within the BrainVoyager environment and were used for the preprocessing of the TRACK-PD study data. The data of the fMRI bladder state study was preprocessed mostly manually, involving the same steps. The scripts are included in the Appendix A. Figure 8 illustrates all the steps applied to the data to complete preprocessing and identifies the specific automatic Python scripts for each preprocessing step of the TRACK-PD data.

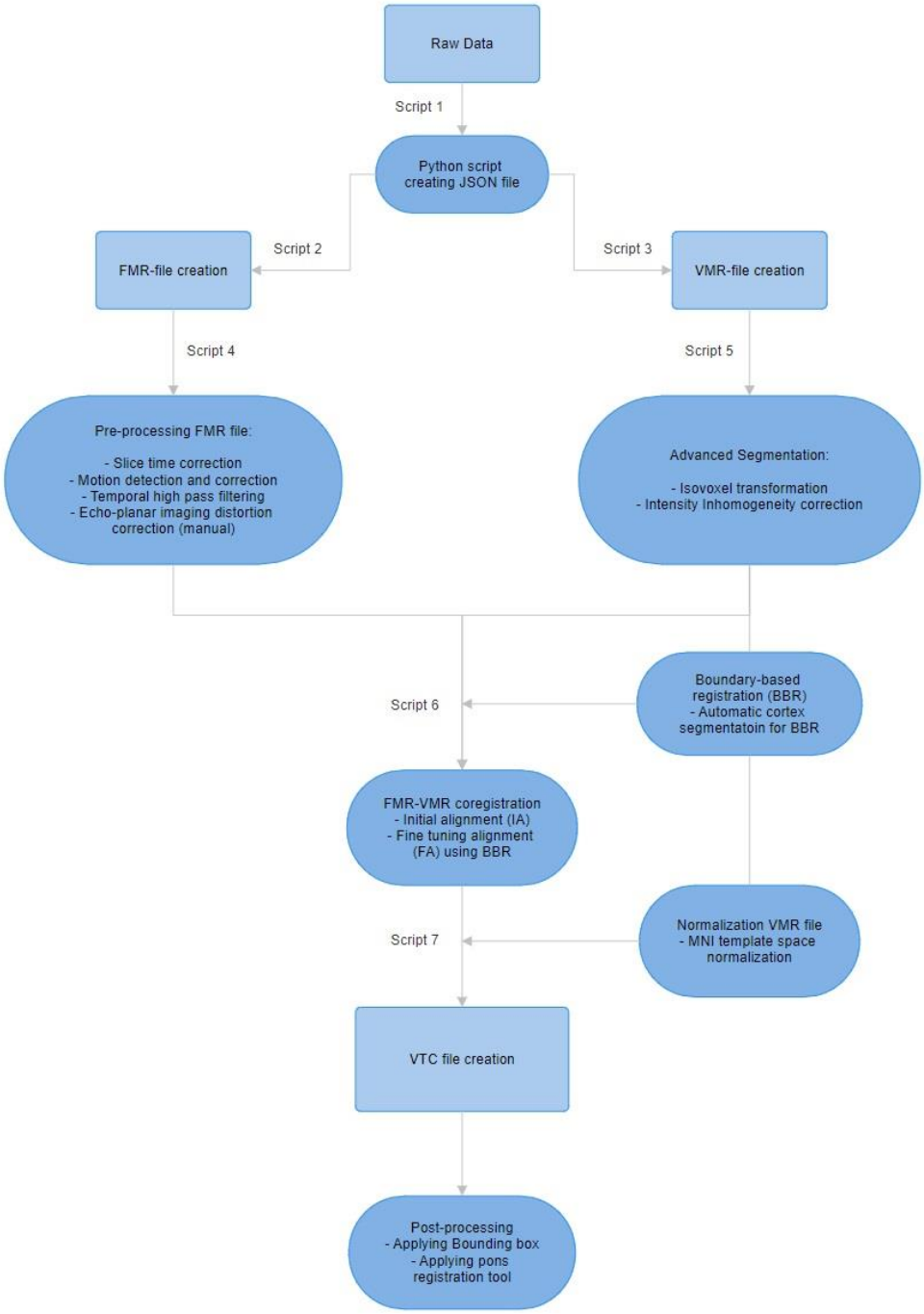

Figure 8: The preprocessing workflow. General overview of all the steps applied to the raw data

Functional data

For the TRACK-PD data, an extra Python script was used to extract relevant information, including the names of the data files (such as the fMRI data, the anatomical data, and the phase encoding data), the name of the first volume, the DICOM file number, the number of volumes, and the number of slices. This information was then stored in JSON files (Script 1), ensuring that the correct data was selected for further preprocessing steps. The first step in preprocessing the functional data involved converting the data into FMR files for each subject using BrainVoyager (Script 2). These FMR files were subsequently preprocessed using slice timing correction, motion correction, and temporal high-pass filtering (Script 4):

- *Slice Time Correction:* Functional volumes are acquired one slice at a time. During a set repetition time (TR), a whole volume is acquired. The capture of these slices is therefore spread out over the TR, the time it takes to capture a whole volume. fMRI analysis assumes that all slices are captured at the same time, therefore the data must be preprocessed to appear as if all slices were taken at the same moment in time. To achieve this, the time series of individual slices are temporally shifted to match a certain reference point (Figure 9). This shift is performed by resampling the original data, involving interpolation of values from future and past time points. After this temporal resampling, the slices of a functional volume represent the same time point [11, 45].
- *Motion Correction:* During an MRI scan, it is very likely that some (head) movement of the participant occurs. This causes the position of the brain within functional images to vary over time. To prevent this and to improve data quality, motion correction is applied. This step selects a functional volume of a run as a reference and aligns the other volumes to it. The head movements are described by six parameters: three translation (displacement) parameters (in X, Y and Z direction) and three rotation parameters (around the X, Y and Z axis). These parameters are appropriate for characterizing rigid body movement [46].
- *Temporal High-Pass Filtering:* Voxel time courses often exhibit signal drifts caused by physical (scanner-related) and physiological noise. These drifts could substantially decrease the power of statistical data analysis if not corrected. These drifts describe slow signal changes, which can be removed by Fourier analysis using a temporal high-pass filter. The original time-domain signal is transformed into frequency space using Fourier Transformation. In frequency domain, low-frequency drift can easily be removed. The filtered frequency representation can then be transferred back into the time domain using the inverse Fourier transformation (Figure 10) [11, 47].

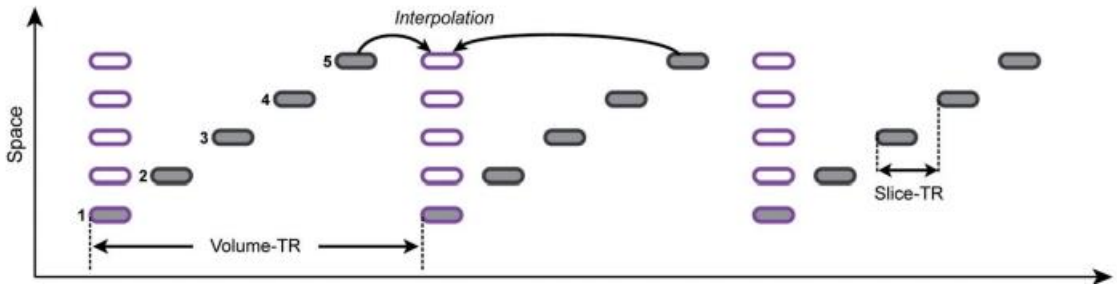

Figure 9: In slice time correction, slices within a volume (represented by black rectangles) are shifted in time to create new time frames (violet rectangles) where the slices of a volume are virtually measured simultaneously. To calculate time points that fall between the actual measured points, interpolation (usually sinc or linear interpolation) is applied. Accurate interpolation requires knowledge of the volume TR, slice TR, and slice scanning order [11].

The last step of the preprocessing of the functional data is the echo-planar imaging (EPI) distortion correction. This step could not be automated by writing a Python script, so it was performed manually using the Opposite Phase Encoding (COPE) plugin in BrainVoyager. Due to static magnetic field inhomogeneities, geometric distortions occur, leading to pixel shifts, especially in the phase encode direction. To correct for these deformations, the COPE plugin utilizes a pair of EPI images, acquired with opposite phase -encoding directions (anterior-posterior and posterior-anterior), to estimate a voxel displacement map. This map shows the degree to which each voxel needs to be transformed back to its original location to correct for field inhomogeneity [48, 49].

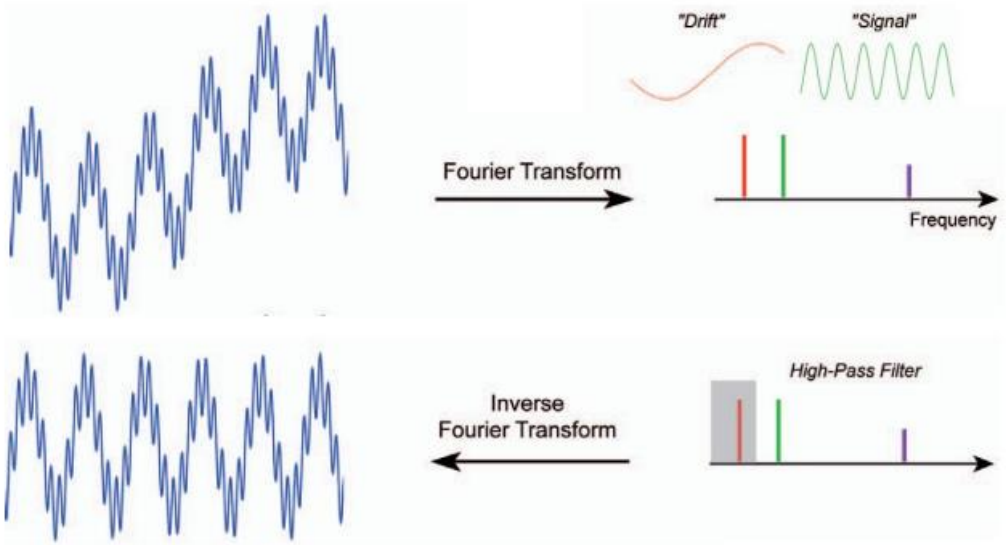

Figure 10: Principle of Temporal High-Pass Filtering using Fourier analysis. In the upper left, the signal in the time domain is shown. This consists of the 'drift' and the real signal. By applying the Fourier Transformation, the data is transformed into the frequency domain. Here, frequencies can be filtered to remove unwanted signal components. In the lower right part, a high-pass filter is applied. This filter removes the lower frequencies, which represent the 'drift'. The frequency domain data can then be transformed back to the time domain by applying the Inverse Fourier Transform [11].

Anatomical data

The first step of the preprocessing of the anatomical data was transforming the data into VMR files for each subject in BrainVoyager (Script 3). The resulting VMR files where then preprocessed by isovoxel transformation and inhomogeneity correction (Script 5):

- *Isovoxel Transformation:* During this step, the data is resampled to a 1.0 millimeter isovoxel using cubic spline interpolation. The data is then placed into a 256 framing box [50, 51].
- *Intensity Inhomogeneity Correction (IIHC):* Inhomogeneity of intensities in the data can reduce the accuracy of segmentation and registration, especially for segmentation tools based on region growing approaches. White matter voxels at one position could have the same intensity as gray matter voxels at other locations in the image. A method which performs well for IIHC uses a 'surface fitting' approach. In this approach, low-order polynomials model low-frequency variations across 3D image space, and are fitted to a subset of voxels belonging to white matter. The low-frequency intensity fluctuations (bias field) are estimated and removed, resulting in more homogeneous voxel intensities. This enhances visualization and provides a better starting point for subsequent segmentation tools. During this step, the brain is extracted from the head tissue, and the white matter in the brain is determined [52].

Co-registration

After the preprocessing of the functional and the anatomical data, the data needs to be aligned. The co-registration of the data is performed by taking the first volume of the functional data and aligning it to the corresponding anatomical data. This alignment is achieved by calculating two transformation matrices: a header-based initial alignment (IA) and a boundary-based registration (BBR) for fine-tuning alignment (FA). This registration method consists of white-gray matter segmentation, reconstruction and smoothing of a white-gray matter mesh, and the final implementation of the BBR algorithm. These steps transform all volumes of the functional data into the anatomical space (Script 6).

VTC-creation

After the co-registration, all the data is transferred to MNI space. This standardizes the data, making it possible to compare it to other data in MNI space. First, the anatomical data is normalized to MNI space using template matching. This registration utilizes affine registration algorithms. These MNI transformation results, together with the IA and FA files, can then be combined into one transformation matrix. This information is then applied to the functional data, transforming it into MNI space (Script 7). This transformation creates a VTC-file, which can then be used for post-processing steps. The VTC file of each subjects contains the functional data of a scan (FMR file) in the space of the 3D anatomical data (VMR), in MNI space [53].

Pons registration tool

The registration of anatomical and functional data to MNI space, performed by BrainVoyager, primarily uses cortical landmarks for normalization, leading to suboptimal alignment of subcortical regions. However, in this research, the ROI lies within the pons. Figure 11 shows that the registration of the pons in MNI space is not yet optimal. This discrepancy partly stems from anatomical variations among subjects (such as variations in pons size) or suboptimal registration accuracy of BrainVoyager in the pons area. Since this research focuses on small regions within the pons, facilitated by UHF fMRI which allows for precise investigation of these areas, accurate registration in MNI space is crucial to enhance research quality.

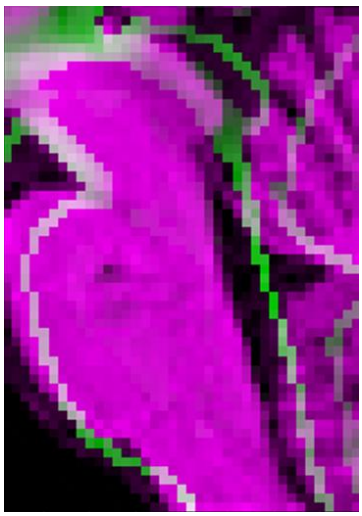

Figure 11: Sagittal view of the pons (including the midbrain, part of the medulla oblongata and cerebellum) of a subject of the TRACK-PD study. The pink part belongs to the VMR data of the subject, while the green outline belongs to the standardized pons in MNI space from BrainVoyager. It can be seen that the registration of the pons in MNI space is suboptimal. Both the ventral and dorsal parts of the pons are inadequately aligned with the MNI space pons

To obtain optimal registration of the anatomical and functional data to MNI space, and to make it more accurate for statistical analysis and better comparability with the other data, a MATLAB tool was developed. First, a bounding box was applied on the VTC data to reduce file size and computation time in subsequent analyses. The pons is the ROI and all data has already been transformed into MNI space by BrainVoyager in a suboptimal way as seen in Figure 11. Due to this transformation to MNI space by BrainVoyager, the pons of every subject is approximately present in the same spatial location, which

makes the pons of every subject being present in our applied bounding box. This serves as an initial alignment, making bounding box application feasible for each subject, encompassing the entire pons, part of the fourth ventricle, medulla oblongata, and midbrain. Additionally, the VMR files (containing anatomical data in MNI space) and the VTC files (containing the functional data in MNI space) for each subject were previously registered in BrainVoyager. The bounding box was then applied to the VMR file containing anatomical data of every subject and to the VMR file of the brain in MNI space provided by BrainVoyager. This application of the bounding box standardized the size of both VMR files. Both VMR files are T1-weighted MRI scans and were normalized/rescaled so all voxel values were transformed to a range between 0 and 1. This normalization step is crucial for subsequent monomodal registration, since this makes use of the MeanSquares similarity metric. Subsequently, the 'imregtform' function in MATLAB was employed to perform the registration between the VMR files, utilizing an intensity based registration algorithm [54, 55]. Affine registration was chosen due to potential variations in pons sizes among subjects, making rigid registration insufficient for optimal pons registration with the MNI pons. Additionally, affine registration algorithms are used in BrainVoyager to register VMR files to MNI space. Affine registration involves transformations such as translation, rotation, scaling, and shearing. This registration yielded a transformation matrix for each subject. To quantify the result of the registration, the Mean Squared Error (MSE) was calculated between the fixed volume (MNI pons) and the moving volume (pons of the subject before registration) as well as between the fixed volume and the registered volume (pons of the subject after registration). MATLAB automatically minimizes the MSE during the registration process, thereby optimizing the alignment between the fixed and moving volumes. Since the data was not normally distributed, the difference in MSE before and after registration was assessed using the Wilcoxon signed rank test. These results are detailed in the 'Results' section. The final step involved applying the resulting transformation matrix to the VTC data (functional data) for each subject. Thus, a transformation matrix was calculated for each subject and subsequently applied to their corresponding VTC data. The MSE was calculated for all subjects of the TRACK-PD study population who were included in this study.

Post-processing

The post-processing steps were conducted in MATLAB 2023a. In this research, four groups were considered: subjects from the TRACK-PD study suffering from PD formed one group (N=31). The healthy controls from the TRACK-PD study formed the second group (N=17). Subjects from the fMRI bladder state study involving an empty bladder scan formed the third group (N=7), and subjects from the fMRI bladder state study involving a full bladder scan formed the fourth group (N=7).

Since both datasets were transformed into MNI space, and this registration was optimized using the pons registration tool, masks in MNI space were employed to compare specific subregions within the pons. For this research, masks encompassing the pons and Bar were utilized. These masks were developed in earlier research. The pons mask contains 21795 voxels. The mask of Bar consists of 256 voxels and was defined based on findings from two studies [56, 57]. The study of Blanco et al. detailed the anatomical location of Bar relative to the LC using histological staining, while the study of Keren et al. mapped the location of the LC in MNI space. The mask of Bar was drawn manually in MNI space using BrainVoyager, based on the information in these articles. The masks of the pons and Bar that were used for these calculations are shown in Figure 12.

In all four groups, the mean fMRI signal was calculated within Bar using the mask of Bar. This signal was then correlated with the BOLD signal of every voxel within the pons (excluding Bar) using the pons mask. This resulted in correlation maps between Bar and every voxel in the rest of the pons for all subjects. This analysis was performed across all subjects in the four groups, and the correlation coefficients were normalized using the Fisher's Z-transformation. Then, for all four groups, the mean was taken of all the correlation maps of the subjects in each group. This resulted in four average group correlation maps: namely of the healthy controls from the TRACK-PD study, the PD patients from the TRACK-PD study, the

subjects from the fMRI bladder state study involving an empty bladder scan, and subjects from the fMRI bladder state study involving a full bladder scan. Subsequently, similarities in these maps were qualitatively examined, in a non-automated manner.

For newly identified ROIs, these areas were segmented using ITK-Snap. These segmented areas were used as masks to calculate the mean fMRI signal of this new ROI. This mean signal was correlated with the mean signal of Bar. Next, this calculated correlation between the new ROIs and Bar was investigated for different groups. One comparison involved the empty bladder scan group and the full bladder scan group from the fMRI bladder state study. To assess the difference in correlation between new ROIs and Bar between empty bladder state group and the full bladder state group, the Wilcoxon Rank Test was employed. Another comparison involved PD patients with or without LUTS. This division was based on the MDS-UPDRS questionnaire regarding urinary problems. The first group included PD patients scoring ≥2 on this scale (N=8), while the second group comprised PD patients scoring 0 on this scale (N=11). For both groups, average correlation maps were made. Then, the correlation between Bar and the new ROI was compared between these groups and statistically analyzed using the Wilcoxon rank sum test.

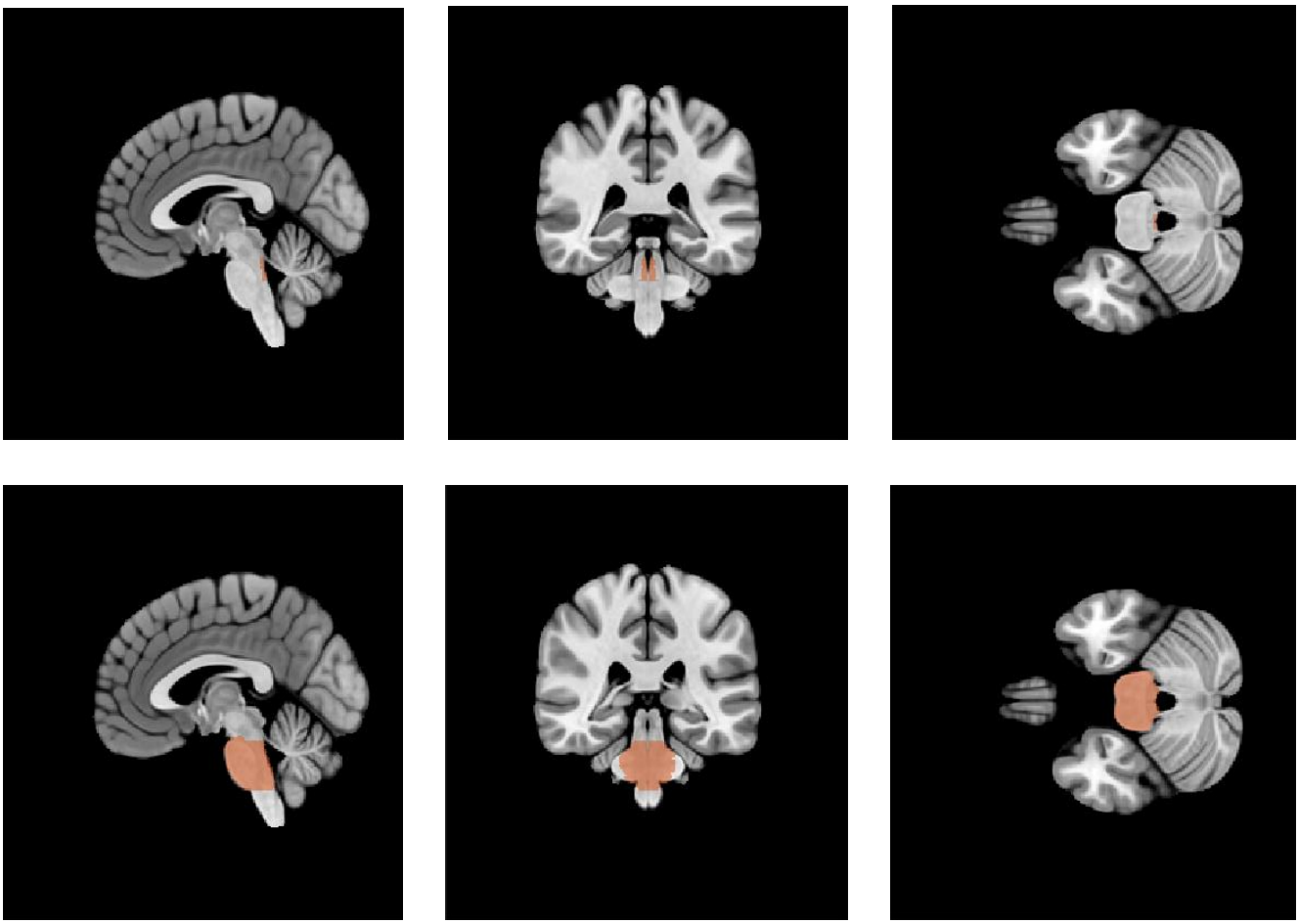

Figure 12: MNI space localization of the masks of Barrington's nucleus and the pons. The first row represents the mask of Barrington's nucleus and the second row represents the mask of the pons in sagittal, coronal and transversal view.

Pons registration tool

The Mean Squared Error (MSE) was determined before and after registration using the pons registration tool. The MSE was calculated based on the VMR file of each subject's pons and the VMR file of the pons in MNI space provided by BrainVoyager. These results are shown in Table 3 of each included subject of the TRACK-PD study. The mean MSE of all subjects before registration was 0.0556, and the mean MSE after registration was 0.0148, which is a significant difference ($p<0.005$). The visual performance of the pons registration tool is provided in Appendix B.

	Mean Square Error (MSE)	
	Before registration	After registration
TRACK-P001	0.0572	0.0211
TRACK-P003	0.0578	0.0182
TRACK-P004	0.0515	0.0163
TRACK-P005	0.0399	0.0128
TRACK-P006	0.0730	0.0122
TRACK-P007	0.0588	0.0070
TRACK-P016	0.0646	0.0104
TRACK-P018	0.0382	0.0153
TRACK-P019	0.0490	0.0078
TRACK-P022	0.0702	0.0152
TRACK-P023	0.0566	0.0173
TRACK-P025	0.0434	0.0183
TRACK-P026	0.0729	0.0198
TRACK-P028	0.0629	0.0089
TRACK-P031	0.0473	0.0155
TRACK-P033	0.0776	0.0235
TRACK-P034	0.0531	0.0179
TRACK-P038	0.0675	0.0177
TRACK-P039	0.0587	0.0094
TRACK-P041	0.0418	0.0109
TRACK-P043	0.0475	0.0196
TRACK-P045	0.0564	0.0135
TRACK-P046	0.0508	0.0175
TRACK-P080	0.0768	0.0204
TRACK-P110	0.0429	0.0174
TRACK-P111	0.0942	0.0111
TRACK-P112	0.0317	0.0113
TRACK-P113	0.0411	0.0103
TRACK-P115	0.0591	0.0117
TRACK-P116	0.0408	0.0165
TRACK-P117	0.0670	0.0087
TRACK-P118	0.0445	0.0118
TRACK-P119	0.0459	0.0157
TRACK-P121	0.0528	0.0206
TRACK-P122	0.0467	0.0173
TRACK-P124	0.0403	0.0157
TRACK-P125	0.0723	0.0167
TRACK-P126	0.0652	0.0191
TRACK-P127	0.0529	0.0185
TRACK-P130	0.0738	0.0083
TRACK-P135	0.0683	0.0112
TRACK-P136	0.0437	0.0155
TRACK-P138	0.0580	0.0125
TRACK-P140	0.0521	0.0098
TRACK-P143	0.0432	0.0104
TRACK-P146	0.0641	0.0213
TRACK-P147	0.0470	0.0100
TRACK-P148	0.0501	0.0209
Mean ± SD	**0.0556 ± 0.0129**	**0.0148 ± 0.0043**

Table 5: the mean square error (MSE) values before and after application of the pons registration tools using the TRACK-PD subjects. Below the mean values and SD of the MSE of both groups are shown.

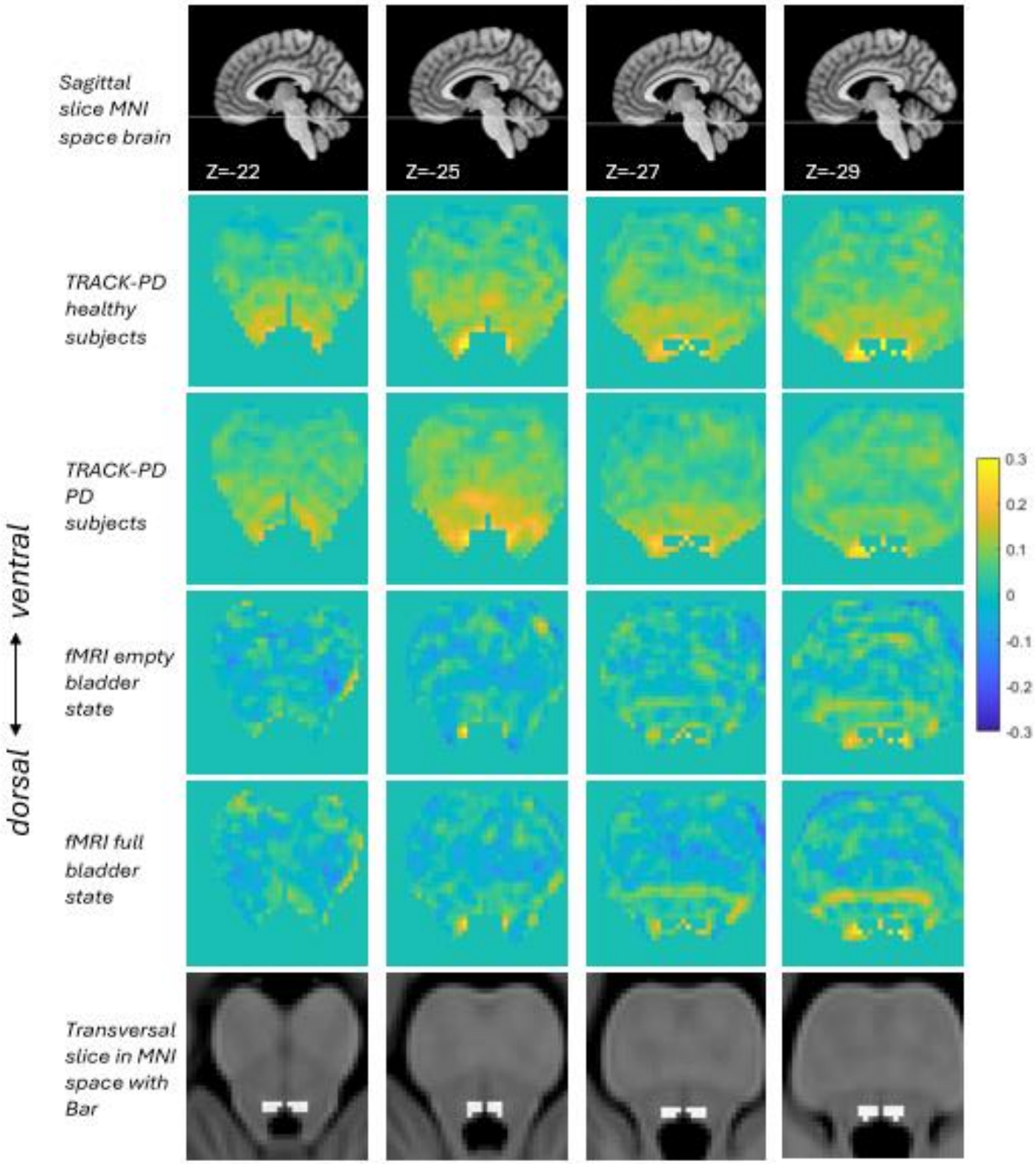

Figure 13: Average correlation maps displaying the correlation coefficients between the mean fMRI signal of Bar and every voxel in the rest of the pons for each group. The first row shows a sagittal view of the brain, indicating the location of the transversal slice within the corresponding column. The second, third and fourth row show four different transversal slices of these average correlation maps of the upper part of the pons for the following groups: the healthy subjects from the TRACK-PD data, the PD subjects from the TRACK-PD data, the fMRI data during an empty bladder, and the fMRI data during a full bladder respectively. The sixth row shows the corresponding transversal slice of the pons in MNI space, with Bar highlighted in white.

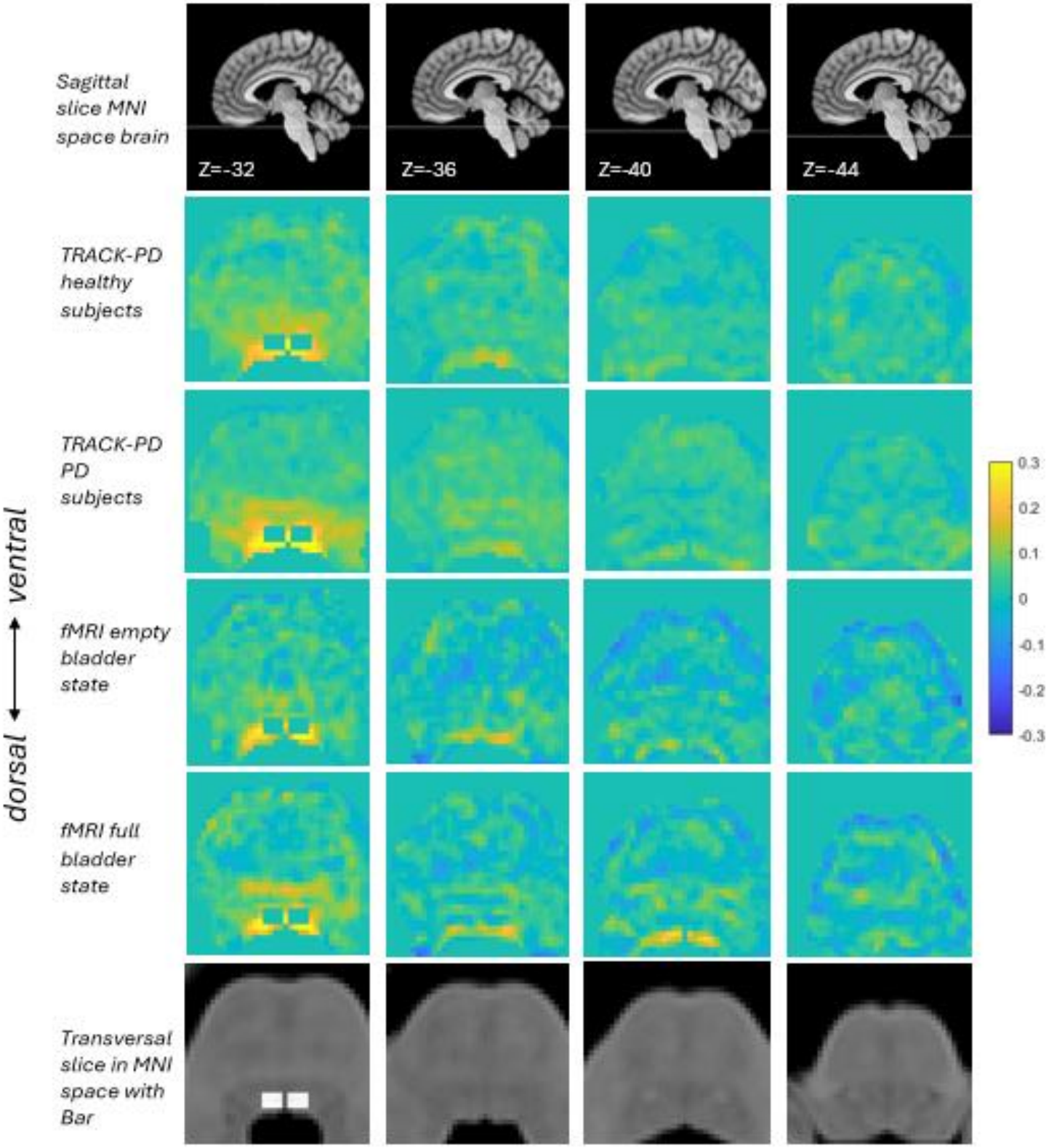

Figure 14: Average correlation maps displaying the correlation coefficients between the mean fMRI signal of Bar and every voxel in the rest of the pons for each group. The first row shows a sagittal view of the brain, indicating the location of th e transversal slice within the corresponding column. The second, third and fourth row show four different transversal slices of these average correlation maps of the lower part of the pons for the following groups: the healthy subjects from the TRACK-PD data, the PD subjects from the TRACK-PD data, the fMRI data during an empty bladder, and the fMRI data during a full bladder respectively. The sixth row shows the corresponding transversal slice of the pons in MNI space, with Bar highlighted in white.

Average correlation maps

The correlation between Bar and the rest of the pons was determined for four different groups: the TRACK-PD group containing healthy subjects, the TRACK-PD group containing PD subjects, the fMRI bladder state subjects during empty bladder state and the fMRI bladder state subjects during full bladder state. For every subject in each group, a correlation map was generated. Then, the mean of the correlation maps of all subjects for every group was calculated which resulted in four average correlation maps. Different transversal slices of these maps are shown in Figures 13 and 14.

As seen in Figures 13 and 14, the medial and lateral area around Bar is highly correlated with Bar in the average correlation maps of all the four groups. This area is most pronounced lateral to Bar rostral in the pons, and dorsal to Bar in the more caudal parts. In the TRACK-PD average correlation map from healthy subjects, this area is located between Z=-22 and Z=-35 using MNI-coordinates. In the PD patients this area is located between Z=-22 and Z=-33. In the fMRI empty bladder state average correlation map between Z=-25 and Z=-37, and in the fMRI data full bladder state average correlation map between Z=-24 and Z=-42.

In addition, a band-shaped region, hereafter referred to as the B-band, was identified in all four average correlation maps, exhibiting relatively high correlation with Bar. This region is located at the border of the tegmentum and basilar pons and is observed across all four average correlation maps, with the most pronounced finding in the fMRI full bladder state group. Segmentation of the B-band was performed using ITK-snap, based on the average correlation map derived from the fMRI full bladder state scan. The segmentation is shown in Figure 15. This segmented B-band was used for subsequent analyses.

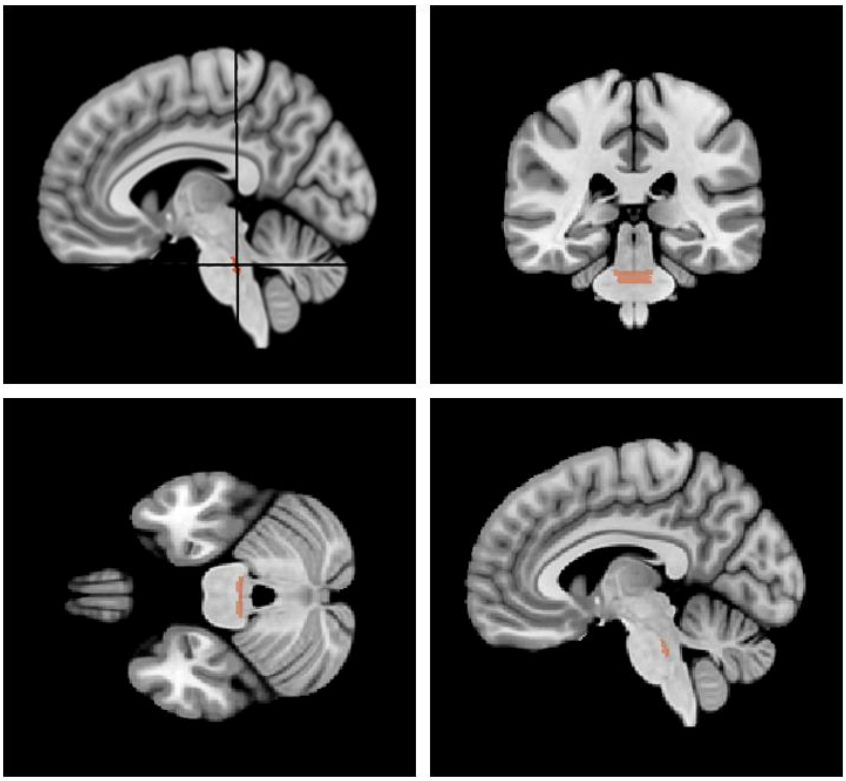

Figure 15: Segmentation of the B-Band shown in the brain in MNI space. The top left figure illustrates the B-Band in orange in sagittal view, showing the location of the transversal and coronal slices. The top right figure represents the brain and the B-Band in a coronal view, the bottom left figure shows the transversal view, and the bottom right figure shows the sagittal view again without the location of the other slices.

The mean fMRI signal across voxels in the B-band was computed and correlated to the mean fMRI signal in Bar for two groups of the fMRI dataset; the fMRI empty bladder state group and the fMRI full bladder state group. Fisher's Z-transformation was applied to the correlation coefficients to obtain Z-scores, facilitating more accurate comparisons between the correlations (see Table 6). A significant difference in the Z-scores was found between these groups (p=0.0469). Thus, the correlation between the B-band and Bar is significantly higher in the fMRI full bladder state group, compared to the fMRI empty bladder state group.

Subjects from fMRI bladder state study	**Z-score fMRI empty bladder state subjects**	**Z-score fMRI full bladder state subjects**
OAB patient 1	0.6747	0.8613
OAB patient 2	0.5801	0.8858
Healthy control 1	0.0422	0.2645
Healthy control 2	0.5033	0.6492
Healthy control 3	0.2877	0.3013
Healthy control 4	0.1441	0.0665
Healthy control 5	0.1903	0.3788

Table 6: Z-scores of the correlation coefficients between Bar and the B-band for the fMRI empty bladder state and full bladder state subjects

The difference in the correlation between the B-band and Bar was also investigated between PD patients with or without LUTS. These results are shown in Table 7, however no significant difference was found between these groups (p=0.8404).

Subjects with LUTS	**Z-score PD subjects**	***Subjects without LUTS***	**Z-score PD subjects**
TRACK-P007	0.0953	*TRACK-P024*	0.8279
TRACK-P031	0.5210	*TRACK-P033*	0.5021
TRACK-P034	0.3407	*TRACK-P039*	0.7532
TRACK-P046	1.1053	*TRACK-P041*	0. 3190
TRACK-P113	0.6670	*TRACK-P110*	0.3339
TRACK-P115	0.3456	*TRACK-P112*	0.4788
TRACK-P118	0.2244	*TRACK-P119*	0.9163
TRACK-P137	0.3985	*TRACK-P122*	-0.0230
		TRACK-P124	0.3373
		TRACK-P130	0.2802
		TRACK-P136	0.2719

Table 7: Z-scores of the correlation coefficients between Bar and the B-band for PD subjects with or without LUTS.

Discussion

In this study, functional activity and connectivity patterns between Bar and the rest of the pons have been investigated using UHF fMRI scans. For this, two datasets have been used: one dataset containing a larger sample size, without a determined bladder state, including healthy subjects and PD patients, and one dataset containing a smaller sample size with subjects during different bladder states (empty and full bladder). The registration of the brainstem in MNI space was optimized by development of a pons registration tool, which improved the registration significantly ($p=<0.005$). The investigation of functional connectivity patterns between Bar and the rest of the pons resulted in four average correlation maps, using the healthy subjects and PD patients of the TRACK-PD data, and the subjects from the fMRI bladder state study during the empty bladder state and the full bladder state. These maps showed a region surrounding Bar with a relatively high correlation with Bar. Furthermore, a new found ROI, called the B-band, was found in all four average correlation maps. The correlation between the B-band and Bar seemed the most profound in the fMRI full bladder state data, which was statistically confirmed ($p=0.0469$). This finding supported our hypothesis that differences will be found in the interaction between Bar and highly correlated areas within the pons, based on bladder state. The correlation between the B-band and Bar did not seem to be different between PD patients with or without LUTS in the TRACK-PD data ($p=0.8404$). This finding was not in accordance with our hypothesis that the interaction between Bar and highly correlated areas within the pons differ based on the presence of LUTS in PD patients.

The registration of the whole brain to MNI space often gives suboptimal results in the brainstem [15]. This is because registration tools often focus on cortical regions instead of the brainstem. Especially for fMRI studies involving the brainstem, optimal registration is critical to improve the quality of the analyses. A reason for this is the close proximity of brainstem nuclei with completely different functions compared to the cortex. Many functional systems are represented by one or more nuclei in the brainstem, resulting in strong functional heterogeneity. The pons registration tool significantly improved the registration of the pons to MNI space. This will improve the quality of the research, since the areas in the pons of all subjects become more reliable and comparable with this improved registration to MNI space. Therefore, the subareas of the pons between all subjects will be more similar, which makes it more feasible to use masks based on MNI-space localization [15].

The average correlation maps of the four groups were examined in a non-automated manner. The focus was on areas that showed relatively high or low correlation coefficients at similar locations in all four maps. Figures 13 and 14 show an area around Bar which is relatively highly correlated with Bar in all four maps. This could partly be due to inaccuracies in registration, causing the coordinates of Bar to be shifted by a few millimeters for some subjects, resulting in high correlations in de average correlation maps surrounding Bar. However, Bar is located medially from LC and laterally from LDTg (Figure 16) [57]. A large part of this highly correlated area is probably LC, which is located more lateral to Bar in the rostral part of the pons, and the more caudal part of LC is located dorsal to Bar. This can also be seen in the average correlation maps. In MNI space, LC is located between Z=-18 and Z=-33 [56]. Especially the highly correlated area around Bar in the TRACK-PD study corresponds to the MNI location of LC. The areas from the fMRI bladder state study seem to be located more caudally. This could be due to some inaccuracies and the smaller sample size. In the literature, it is described that the LC is involved in micturition through its noradrenergic pathways, which influence bladder function via adrenoceptors [9]. Additionally, it was found that noradrenergic neurons in the LC are activated by visceral stimuli such as bladder distension and modulate arousal and attention. Thus, bladder distension activates the LC, which communicates with the cortex, increasing sensory alertness and arousal [9, 21, 58]. Therefore it is thought LC affects micturition indirectly, also possibly by communicating stress-related signals to Bar [8, 59]. The literature

is inconsistent in its use of Bar, PMC and which areas it exactly involves. The PMC is often referred to as a functional concept including Bar and sometimes neurons of the LC and/or LDTg [8].

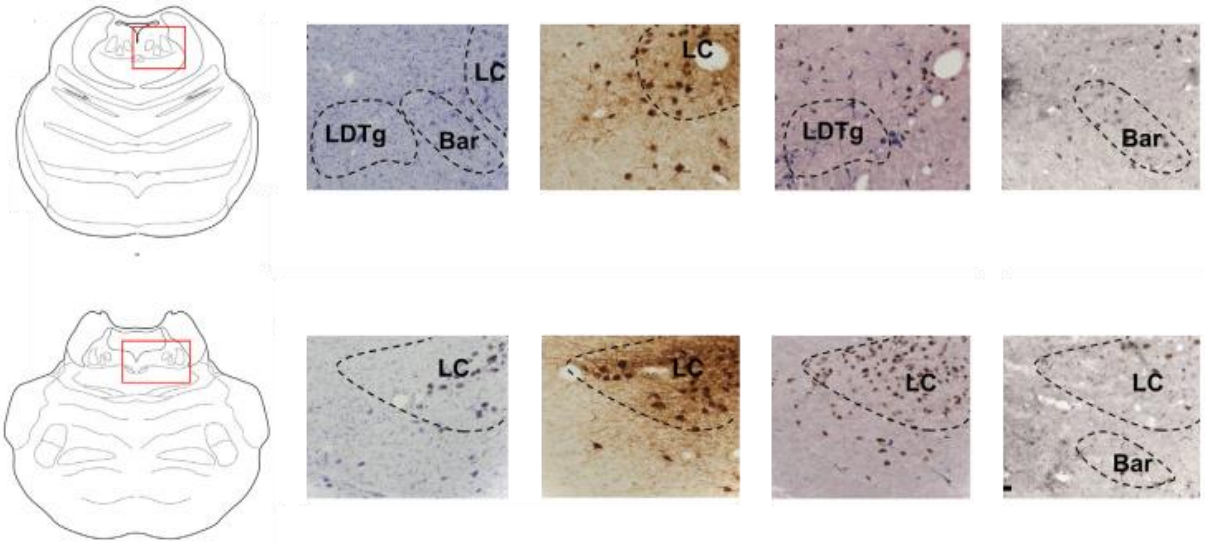

Figure 16: Histological analysis of Barrington's nucleus (Bar) and LC (locus coeruleus) in the human midbrain region. A) shows a transversal slice of the rostral part of Bar in the brainstem. B) shows a transversal slice of the caudal part of Bar in th e brainstem. The figures next to it shown the locations of Bar, LC and laterodorsal tegmental nucleus (LDTg) using different staining techniques [57].

Figures 13 and 14 illustrate the B-band, located at the border of the tegmentum and basilar pons. In MNI coordinates, it stretches from Z=-26 to Z=-35. In the X-direction, the maximum length was X=12 to X=-10. As hypothesized, the B-band and Bar exhibited a significantly higher correlation during the full bladder state compared to the empty bladder state. This indicates that the B-band and Bar interact more during a full bladder state. This increased interaction during full bladder state implies that the B-band may play a role in the micturition pathways. Notably, the highest correlations were found in OAB patients, regardless of bladder state, as seen in Table 4. This could suggest that Bar and the B-band have greater interaction in OAB patients compared to healthy controls.

While it was hypothesized that the correlation between the B-band and Bar would differ depending on the presence of LUTS in PD patients, no significant difference was observed. This was hypothesized since Bar is such an important area within the micturition pathway, that this area could be affected in the interaction with other areas in the presence of LUTS due to PD (see Figure 5). The presence or absence of LUTS in PD patients is therefore probably not a result from differences in interaction between B-band an Bar. As seen in Figure 5, the PMC is not directly influenced by the loss of dopamine due to PD. First, the striatum will be affected, which will affect the PAG and then the PMC. The indirect nature of dopamine's influence on micturition (and LUTS), might be a reason no significant difference were found.

It is not directly clear to which known neuroanatomical location the B-band corresponds to. Three possible neuroanatomical locations will be considered: the PSC, the pontocerebellar fibers and the medial lemniscus. The reasons why the B-band could correspond to each of these suggestions will be elaborated further.

In close proximity of the PAG and Bar, evidence has been acquired that a third brainstem center is involved in LUT control, called the PSC or L-region. It is supposed to be located ventral and lateral of Bar, located in the pontine tegmentum (Figure 17) [29, 60]. In cats, excitation of this region would be involved in the storage of urine, by contracting the pelvic floor muscles and increasing the urethral pressure [9, 30, 32]. In the animal study involving cats by Griffiths et al., bilateral lesions around the L-region could disable the storage of urine, causing detrusor overactivity and severe incontinence [32]. Additionally, this study found that the L-region is part of a larger, more diffuse and less specific area.

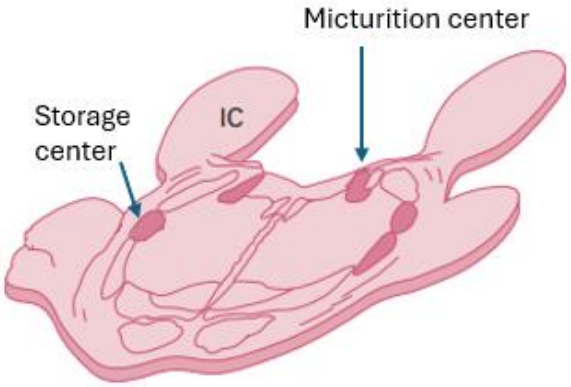

Figure 17: Schematic view of the location of the micturition center (Bar) and the storage center (L-region) in the pons [29] .

Stimulation (over a larger area compared to Bar) gave varying sphincter responses. It has been suggested that the L-region coordinates the response of the urethral sphincter and pelvic floor muscles to different events, such as respiration, sneezing, coughing, vomiting, sexual activity, and potential incontinence. In that case, stimulation of this L-region would lead to varied and less specific responses, depending on the stimulation of the specific part in the L-region. These varied responses were indeed observed in the study of Griffiths et al. in cats [30, 32]. Evidence for the existence of the PSC in humans was found in PET-related research from Blok et al [33, 34]. During this research, subjects were told to void during the PET-scan, so activity in specific areas could be detected in the brain during voiding. In subjects that were unable to void during the scan despite trying, not the area of the Bar lit up, but an area ventrolateral to this area. This area was similar to the expected location of the PSC based on its location in cats [29]. The peak activation (X = +8, Y = -28, Z = -28) of this area falls within the B-band in our study [33]. The PSC, the L-region, is also called the pelvic floor stimulating center. Stimulation in this center activates the pelvic floor via Onuf's nucleus, including the bulbocavernosus, ischiocarvernosus muscles and the EUS [60]. In this research it was found the B-band was significantly higher correlated with Bar during a full bladder state, compared to an empty bladder state. This could mean that in response to a fuller bladder, the B-band would be activated more in order to tighten the urethral sphincter to prevent incontinence. This could also explain why the found correlations are higher in the OAB patients, since they experience more urgency complains which could result in earlier and more sphincter contraction and therefore a higher correlation of this area with Bar. In the literature the PSC is located in the tegmentum, more ventral and lateral to Bar [29]. However, it has not been described that is has a band shaped form. In the study involving the stimulation of the L-region in cats, a diffuse, not specific area was found, however a band shaped area was not described [30]. Our new found B-band could correspond to earlier research describing the PSC, however the band shape form was never mentioned.

The other two possible corresponding neuroanatomical locations are both white matters tracts. Traditionally, fMRI is mostly used for analyzing gray matter, where it detects changes in blood oxygenation related to neural activity. The use of fMRI to investigate white matter gives some challenges. Historically, fMRI was considered less effective for white matter analysis due to the lower cerebral blood volume and flow, which are three to seven times lower compared to gray matter. This reduction in blood flow could make detecting changes in BOLD signals more difficult. Additionally, fMRI signals are believed to originate from post-synaptic potentials, which are more prevalent in gray matter, while white matter predominantly contains axonal fibers and is less involved in these types of potentials since it primarily relies on spiking activity. Despite these challenges, there is no direct evidence against measuring fMRI activation in white matter [61]. Investigations have been performed successfully in the corpus callosum, and functional connectivity within white matter tracts [62, 63]. White matter depends primarily on spiking activity, which contributes minimally to its energy demands. Despite this, it has been demonstrated that white matter

has sufficient vascular capacity to support hemodynamic changes detectable by fMRI, especially at higher magnetic field strengths. Astrocytes might play a role in linking the spiking activity to hemodynamic responses through potassium regulation mechanisms. These cells, along with oligodendrocytes, possess K+ channels that help manage extracellular potassium levels, potentially influencing blood flow and enabling fMRI detection of white matter activity [61].

The B-band could correspond to the pontocerebellar fibers. The cerebral cortex is connected to the cerebellum via cerebropontocerebellar tracts. Corticopontine fibers arise from different areas of the cerebral cortex (mainly from the frontal lobe) and project to the pontine nuclei, located in the basilar pons. From here, fibers project via the middle cerebellar peduncle to the opposite cerebellum via de pontocerebellar fibers [60, 64]. The pontocerebellar fibers are divided into three layers 1) the superficial layers located anteriorly to the pyramidal tract and pontine nuclei; 2) the intermediate layers which separate the bundles of the pyramidal tract and the deep layer, and 3) the deep layer located ventral to the medial lemniscus [10, 64]. As seen in Figure 18, the pontocerebellar fibers have a band-shaped form looking at the transversal slice of the middle of the pons [65]. The review article of Bastide et al. from 2020 gives a clear overview of studies suggesting that the cerebellum modulates the micturition reflex and is involved in the bladder sensory-motor information processing [66]. This review includes experimental animal studies, mostly performed using cats and dogs. These studies showed that electrical stimulation of the cerebellar fastigial nucleus in cats can alter bladder reflexes [67, 68]. Another study showed changes occur in urodynamic parameters after cerebellectomy in dogs [69]. The review article also lists neuroimaging studies that show cerebellar activation during bladder filling or during different bladder states [70, 71]. Additionally, the cerebellum is activated during pelvic floor control in both voluntary and autonomic motor activities [72]. In addition, it shows studies involving clinical observations in humans with cerebellar disorders, such as cerebellar ataxia, which are associated with urinary dysfunction [73, 74]. Patients with cerebellar disorders often have complaints of urgency, frequency, and incontinence, suggesting that the cerebellum plays a role in normal bladder control in humans. Dietrichs et al. suggested some neural projections have been found between Bar and the cerebellum [75]. Therefore, the identified B-band may correspond to the pontocerebellar fibers and possibly pontine nuclei. The pontocerebellar fibers originate from the pontine nuclei and project via the middle cerebellar peduncle to the cerebellum. This B-band is located at the border of the tegmentum and basilar pons, which could correspond to the deep layer of the pontocerebellar fibers which are involved in micturition and/or pelvic control.

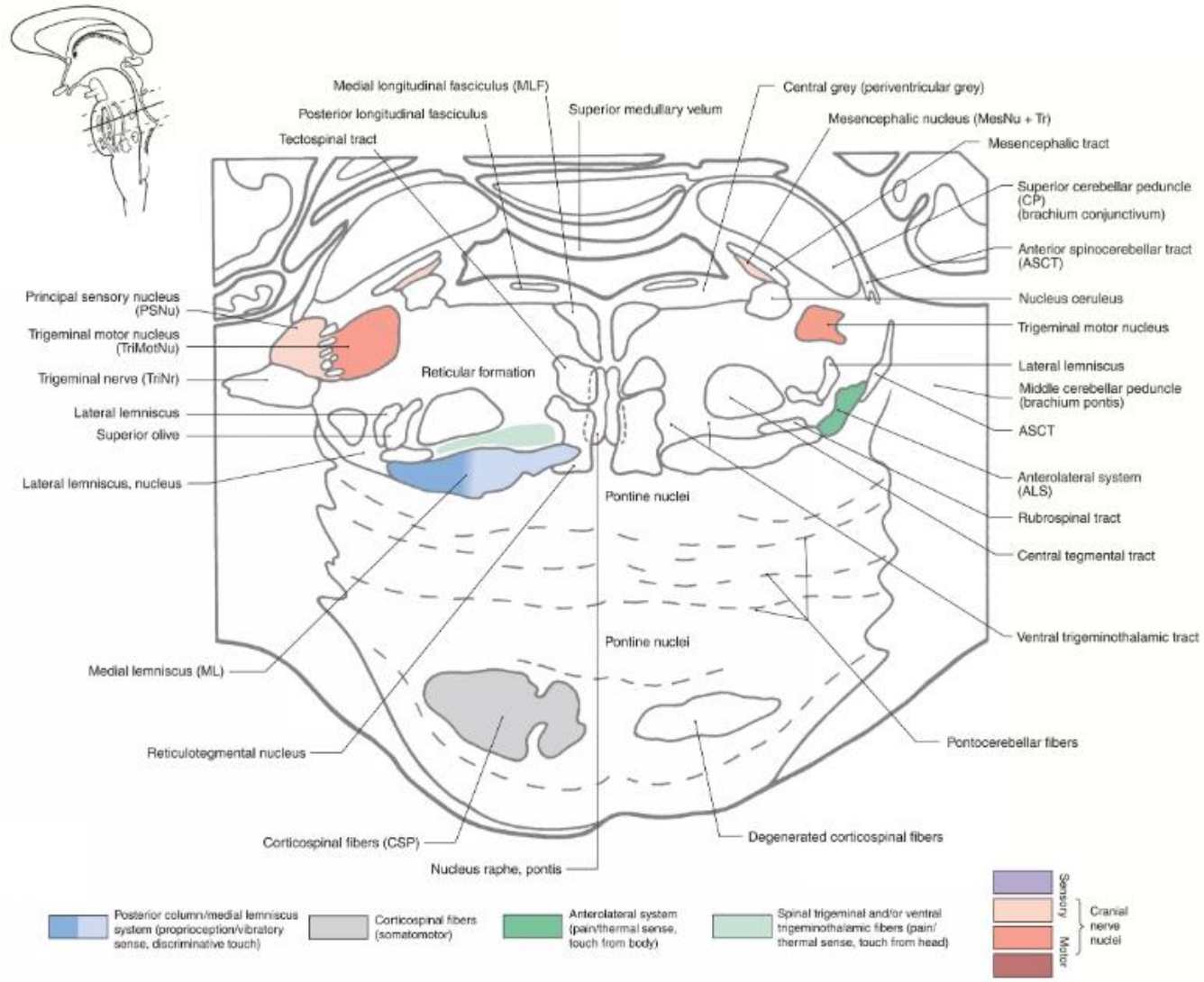

Figure 18: schematic overview of the internal morphology of a transversal section of the pons. In this figure, the ventral part of the pons is below and the dorsal part is at the top. At the border of the tegmentum and the basilar pons the medial lemniscus is located. The pontine nuclei and pontocerebellar fibers can also be seen around this location in the basilar pons [65].

The B-band could also correspond to the location of the medial lemniscus. The medial lemniscus is a second order neuron of the dorsal column medial lemniscus pathway (DCML). It transports the sensory spinothalamic information of conscious proprioception, fine touch, vibration and two-point discrimination of joints and skin of the body and head. The medial lemniscus starts at the nucleus gracilis and cuneatus at the caudal medulla. Then, the tract goes via the caudal medulla, to the ventral posterolateral nucleus of the thalamus, eventually to the primary somatosensory cortex [76, 77]. The trajectory of the medial lemniscus through the pons can be seen in Figure 19 [78]. In the transversal slice in Figure 18, the band shape of the medial lemniscus can be seen, which corresponds to the shape of the B-band. Although the medial lemnisci are not connected to each other in the medial part. In addition, the medial lemniscus is not known to be a part of the neural micturition pathways, since it is involved in the transmission of sensory information of fine touch, proprioception, and vibration sensations. Moreover, as seen in Figure 19, the medial lemniscus runs through the entire brainstem, but our B-band is only present in a portion of the pons.

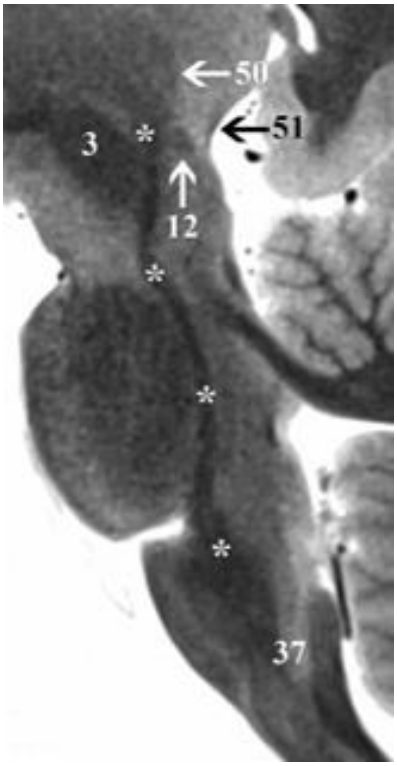

Figure 19: Sagittal section of the brainstem showing the course of the medial lemniscus with an asterisk [78]

The study of Schott et al. investigated the activation in the brain and the brainstem during the initiation of voiding in healthy male and female subjects using 7T fMRI [79]. In Figure 20 (left), a sagittal slice through the middle of the brain is presented, highlighting regions of activation and inhibition associated with voiding. It shows the activation along a tract through the brainstem, potentially corresponding to the medial lemniscus. Additionally, five key regions in the brainstem were found with significant activation or inhibition during voiding (Figure 20, right). One of these regions, indicated by an arrow pointing to the red asterisk in the middle of the pons, corresponds to a location also present within the B-band and was activated during voiding (MNI-coordinates: X = 2, Y = -34, Z = -32).

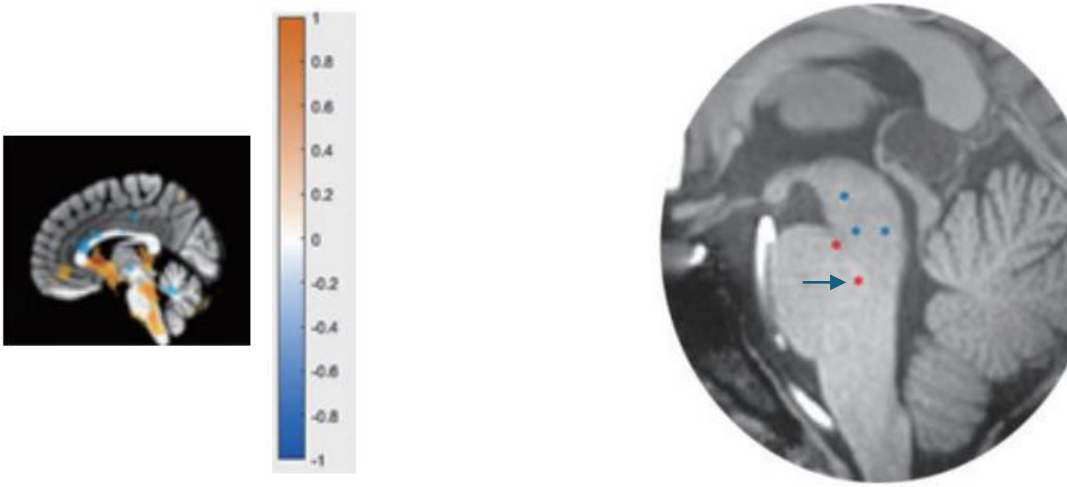

Figure 20: Both figures show a sagittal slice of the brain, which show activation and inhibition of areas during voiding. On the left the whole brain is shown with areas of activation (orange) and inhibition (blue) in both genders during initiation of voiding. On the left figure the five key areas representing activation (red asterisks) and inhibition (blue asterisks) are shown in the brainstem during voiding [79].

Three areas are described which could correspond to the B-band found in this research. However it is worth speculating that some of these regions might represent the same underlying structure. In the study of Blok et al., PET-CT including [15O]H2O was used to capture brain activity during voiding [33]. The L-region or PSC was activated in subjects who were unable to void despite their efforts. The location of the peak activation of this area falls within the spatial extent of the B-band. However, the B-band stretches in transversal direction along the pons, which could anatomically correspond with the pontocerebellar fibers. Given that PET-CT imaging may have reduced accuracy in detecting brain activity in white matter compared to gray matter, it is possible that the PET-CT scan in Blok et al.'s study only captured part of the B-band's activity [33, 80, 81]. This captured activity could correspond to a pontine nucleus, potentially the origin of the pontocerebellar fibers. This research, resulting in the B-band, could involve the same pontine nucleus, including the pontocerebellar fibers projecting to the cerebellum. Therefore, it could be speculated that the PSC is actually a specific pontine nucleus, with projections (the pontocerebellar fibers) to the cerebellum, involved in pelvic control.

Limitations and future perspectives:

The pons registration tool significantly improved the accuracy of the registration of the pons in MNI space, however the accuracy of the tool could be further improved. As seen in Appendix B, still a degree of mismatch exists between the registered pons and the pons in MNI space, especially when the pons of the subject is different in size or has a different shape compared to the MNI pons. In brainstem analyses this can affect the results, since the nuclei in the brainstem are small and functional different nuclei lie in very close proximity to each other. Therefore, small registration errors may still reduce the quality of the analyses [15]. Another way to assess the registration performance, is by segmentation of the fixed volume (the pons in MNI space) and of every moving volume (the pons of every subject). This way a Dice coefficient can be calculated, which measures the spatial overlap between two objects. The Dice coefficient ranges between 0 and 1, where a higher score means more overlap and thus a better registration [82]. The pons registration tool significantly improved the registration of the pons, which is visually demonstrated in Appendix B.

In the fMRI bladder state data all subjects were female. In the TRACK-PD data, most subjects were male (see Tables 2 and 3). This difference could introduce bias due to the differing pathophysiology of LUTS between genders. Benign Prostatic Hyperplasia (BPH) is common in older men and can cause LUTS due to prostatic obstruction which gives obstructive symptoms. Moreover, it may lead to detrusor overactivity (DO) and symptoms such as urgency or incontinence. Therefore, LUTS in older men with PD could partly be attributable to BPH, in addition to being secondary to PD [40, 83]. Next to this, the mean age is different in both datasets. The mean age in the fMRI bladder state data is 39,3 years and 61,1 years in the TRACK-PD data. Ideally, these age differences would be minimized to reduce potential confounding factors related to age differences.

The sample size of the TRACK-PD data was larger compared to the fMRI bladder state data. The results from this dataset are therefore more reliable compared to the results from the fMRI bladder state data, which only consisted of seven subjects. As seen in the average correlation maps in Figures 13 and 14, the maps from the TRACK-PD data seem more smooth and homogeneous, compared to the maps of the fMRI bladder state data. Due to the larger sample size, noise and outliers are cancelled out to a higher degree. Therefore, it would be desirable to increase the fMRI bladder state data, so the analyses can be performed on a larger sample size, resulting in more reliable results. Also the sample size of the TRACK-PD data can be increased. Due to technical difficulties in the automatic preprocessing steps, not all available data of the TRACK-PD data was used. In case these technical difficulties can be overcome, this sample size can be increased as well, which would increase the impact of the found results and make them more reliable.

The use of UHF MRI scanners, combined with advancements in the registration of the pons enhances the feasibility of investigating functional activity and connectivity patterns between regions located in the pons. During this research, the correlation between Bar and the rest of the pons was investigated. However, exploring the functional connectivity patterns between Bar and other subcortical areas involved in micturition, such as the PAG, thalamus, substantia nigra, and LC, could provide valuable insights. The micturition reflex seems to be influenced by dopamine, which is mostly produced by cells in the substantia nigra. Dopamine has an inhibitory effect on the micturition pathway, especially by inhibiting the PAG. The substantia nigra degenerates in PD, which decreases dopamine production. This leads to a loss of the inhibitory functions of dopamine, leading to bladder overactivity. It is thought that the LC also plays a role in this, since dopamine loss leads to less inhibition of noradrenergic pathways via the LC. This all is thought to play a role in the resulting LUTS in PD patients [9, 20]. Therefore, further investigation into the functional connectivity patterns between Bar and the substantia nigra, as well as between Bar and the LC, could yield important findings. In this investigation, it would be interesting to look at the differences between healthy controls and PD patients. Analyzing the interactions between subcortical and cortical areas during different bladder states would also be a significant area of study. Next to this, the investigation of the functional connectivity between PAG and the B-band would be very informative. The PAG is known to be organized in a symmetrical columnar way, where the dorsolateral and ventrolateral parts are indicated to be involved with the storage and voiding of urine respectively [1]. Since the B-band seems to be dependent of bladder state, it would be interesting to investigate whether this B-band has different connectivity patterns with different parts of the PAG, corresponding to the dorsolateral and ventrolateral parts, also during different bladder states.

The corresponding neuroanatomical region to the B-band remains uncertain. The most likely corresponding neuroanatomical region is the PSC or the pontocerebellar fibers, since these areas are most probably located in the area of the B-band and studies suggests their involvement in micturition pathways. Further research is needed to explore this B-band. The correlation between Bar and this B-band was significantly stronger during full bladder state. However, it is not clear whether this is a direct result of differences in bladder state, or due to differences in pelvic control due to a full bladder. Therefore, it would be interesting to investigate the correlation between Bar and the B-band during other bladder states. The fMRI bladder state study also consists of filling bladder scans of each subject, during which the bladder is artificially filled with saline via a catheter. This way the progression of the correlation during the filling of the bladder can be investigated. Additionally, examining the correlation between Bar and this B-band during voiding could provide valuable insights. In particular, comparing the activity of our B-band in subjects unable to void during the scan with those who can void may validate the findings reported by Blok et al. using fMRI [29, 33]. Unfortunately, the fMRI bladder state study does not contain fMRI scans during voiding. Since another possible corresponding neuroanatomical region to the B-band could be the pontocerebellar fibers, it would be interesting to investigate the functional connectivity between Bar and the cerebellum or the B-band and the cerebellum. In order to investigate whether the B-band indeed corresponds to white matter tracts, and to which white matter tracts, Diffusion Tensor Imaging (DTI) can be used [84]. DTI is a form of diffusion-weighted imaging (DWI), and is able to capture the direction and magnitude of water diffusion. DTI measures functional anisotropy (FA), which indicates the direction of the water diffusion in a voxel, resulting in a vector per voxel. DTI can reconstruct pathways of white matter, by following the direction of the vectors. High FA values typically indicate organized white matter tracts, since water diffusion is directionally constrained by the myelin sheaths. Therefore, DTI enables the visualization of neural pathways and connectivity. The TRACK-PD data also consists of DTI imaging (see section 'Methods') which makes it possible to investigate the direction of the B-band and whether it indeed consists of white matter tracts [42, 84].

Conclusion

The present study aimed to investigate the functional activity and connectivity patterns between Bar and the rest of the pons, focusing on the influence of bladder state and the presence or absence of LUTS in PD patients. Two distinct datasets were analyzed for this purpose. An area surrounding Bar was found to be highly correlated with Bar, likely due to its proximity, but it may also correspond to the LC, which is known to be involved micturition pathways. Another area highly correlated with Bar, was identified between the tegmentum and the basilar part of the pons, with a correlation significantly higher during a full bladder state. This so called B-band is likely to be involved in micturition pathways and shows dependency of bladder state. It has a band-shaped appearance, and its location does not correspond directly to a specific neuroanatomical structure. However, based on its location and activity, possible neuroanatomical candidates include the PSC, pontocerebellar fibers, or the medial lemniscus. Further research is needed to explore this area and its role in micturition pathways.

The developed pons registration tool significantly improved the registration of the pons to MNI space. Additionally, the identification of the B-band across two different datasets demonstrates the feasibility of investigating functional activity and connectivity patterns within the pons. This paves the way for other investigations regarding the functional activity and connectivity between regions within the pons or brainstem, which could provide valuable insights into the interaction of different brain regions involved in bladder storage and micturition pathways.

References

1. de Rijk, M.M., et al., *Parcellation of human periaqueductal gray at 7-T fMRI in full and empty bladder state: The foundation to study dynamic connectivity changes related to lower urinary tract functioning.* Neurourol Urodyn, 2021. **40**(2): p. 616-623.
2. Fernandez Chadily, S., et al., *Assessment of Brainstem Functional Organization in Healthy Adults and Overactive Bladder Patients Using Ultra-High Field fMRI.* Biomedicines, 2023. **11**(2).
3. Abrams, P., et al., *The standardisation of terminology in lower urinary tract function: report from the standardisation sub-committee of the International Continence Society.* Urology, 2003. **61**(1): p. 37-49.
4. Leron, E., et al., *Overactive Bladder Syndrome: Evaluation and Management.* Current Urology, 2018. **11**(3): p. 117-125.
5. Vaughan, C.P., et al., *Behavioral therapy for urinary symptoms in Parkinson's disease: A randomized clinical trial.* Neurourol Urodyn, 2019. **38**(6): p. 1737-1744.
6. Brucker, B.M. and S. Kalra, *Parkinson's Disease and Its Effect on the Lower Urinary Tract: Evaluation of Complications and Treatment Strategies.* Urol Clin North Am, 2017. **44**(3): p. 415-428.
7. Fowler, C.J., D. Griffiths, and W.C. de Groat, *The neural control of micturition.* Nat Rev Neurosci, 2008. **9**(6): p. 453-66.
8. Verstegen, A.M.J., et al., *Barrington's nucleus: Neuroanatomic landscape of the mouse "pontine micturition center".* J Comp Neurol, 2017. **525**(10): p. 2287-2309.
9. de Groat, W.C., D. Griffiths, and N. Yoshimura, *Neural control of the lower urinary tract.* Compr Physiol, 2015. **5**(1): p. 327-96.
10. Rahman, M. and A.B. Siddik, *Neuroanatomy, Pontine Micturition Center*, in *StatPearls*. 2024: Treasure Island (FL) ineligible companies. Disclosure: Abu Bakar Siddik declares no relevant financial relationships with ineligible companies.
11. Goebel, R., *Localization of Brain Activity using Functional Magnetic Resonance Imaging*, in *Clinical Functional MRI: Presurgical Functional Neuroimaging*, C. Stippich, Editor. 2007, saSpringer Berlin Heidelberg: Berlin, Heidelberg. p. 9-51.
12. Rogers, B.P., et al., *Assessing functional connectivity in the human brain by fMRI.* Magn Reson Imaging, 2007. **25**(10): p. 1347-57.
13. Friston, K.J., *Functional and effective connectivity: a review.* Brain Connect, 2011. **1**(1): p. 13-36.
14. Mohanty, R., et al., *Rethinking Measures of Functional Connectivity via Feature Extraction.* Scientific Reports, 2020. **10**(1): p. 1298.
15. Beissner, F., *Functional MRI of the Brainstem: Common Problems and their Solutions.* Clin Neuroradiol, 2015. **25 Suppl 2**: p. 251-7.
16. Sclocco, R., et al., *Challenges and opportunities for brainstem neuroimaging with ultrahigh field MRI.* Neuroimage, 2018. **168**: p. 412-426.
17. Jezzard, P., P.M. Matthews, and S.M. Smith, *Functional MRI: an introduction to methods*. Vol. 61. 2001: Oxford university press Oxford.
18. Chau, W. and A.R. McIntosh, *The Talairach coordinate of a point in the MNI space: how to interpret it.* Neuroimage, 2005. **25**(2): p. 408-16.
19. Holstege, G. and H. Collewijn, *Chapter 9 - Central Nervous System Control of Micturition*, in *The Spinal Cord*, C. Watson, G. Paxinos, and G. Kayalioglu, Editors. 2009, Academic Press: San Diego. p. 130-147.
20. Kitta, T., et al., *Animal Model for Lower Urinary Tract Dysfunction in Parkinson's Disease.* Int J Mol Sci, 2020. **21**(18).
21. Malykhina, A.P., *How the brain controls urination.* eLife, 2017. **6**: p. e33219.

22. Yoshimura, N., et al., *Neural Mechanisms Underlying Lower Urinary Tract Dysfunction.* Korean journal of urology, 2014. **55**: p. 81-90.
23. Lee, C.L., et al., *Sophisticated regulation of micturition: review of basic neurourology.* J Exerc Rehabil, 2021. **17**(5): p. 295-307.
24. Feloney, M.P., K. Stauss, and S.W. Leslie, *Sacral Neuromodulation*, in *StatPearls*. 2024, StatPearls Publishing

25. McMahon, S.B. and K. Spillane, *Brain stem influences on the parasympathetic supply to the urinary bladder of the cat.* Brain Res, 1982. **234**(2): p. 237-49.
26. Chen, S.Y., et al., *Glutamate activation of neurons in CV-reactive areas of cat brain stem affects urinary bladder motility.* Am J Physiol, 1993. **265**(4 Pt 2): p. F520-9.
27. Sugaya, K., et al., *Evidence for involvement of the subcoeruleus nucleus and nucleus raphe magnus in urine storage and penile erection in decerebrate rats.* J Urol, 1998. **159**(6): p. 2172-6.
28. Sugaya, K., et al., *Central nervous control of micturition and urine storage.* J Smooth Muscle Res, 2005. **41**(3): p. 117-32.
29. Blok, B.F. and G. Holstege, *The central control of micturition and continence: implications for urology.* BJU Int, 1999. **83 Suppl 2**: p. 1-6.
30. Griffiths, D.J., *The pontine micturition centres.* Scand J Urol Nephrol Suppl, 2002(210): p. 21-6.
31. Holstege, G., et al., *Anatomical and physiological observations on supraspinal control of bladder and urethral sphincter muscles in the cat.* J Comp Neurol, 1986. **250**(4): p. 449-61.
32. Griffiths, D., et al., *Control and coordination of bladder and urethral function in the brainstem of the cat.* Neurourology and urodynamics, 1990. **9**(1): p. 63-82.
33. Blok, B.F., A.T. Willemsen, and G. Holstege, *A PET study on brain control of micturition in humans.* Brain, 1997. **120 (Pt 1)**: p. 111-21.
34. Blok, B.F., L.M. Sturms, and G. Holstege, *Brain activation during micturition in women.* Brain, 1998. **121 (Pt 11)**: p. 2033-42.
35. Kavia, R., et al., *A functional magnetic resonance imaging study of the effect of sacral neuromodulation on brain responses in women with Fowler's syndrome.* BJU Int, 2010. **105**(3): p. 366-72.
36. Tadic, S.D., et al., *Brain activity underlying impaired continence control in older women with overactive bladder.* Neurourol Urodyn, 2012. **31**(5): p. 652-8.
37. Kuhtz-Buschbeck, J.P., et al., *Activation of the supplementary motor area (SMA) during voluntary pelvic floor muscle contractions--an fMRI study.* Neuroimage, 2007. **35**(2): p. 449-57.
38. Griffiths, D., *Neural control of micturition in humans: a working model.* Nat Rev Urol, 2015. **12**(12): p. 695-705.
39. Kavia, R.B., R. Dasgupta, and C.J. Fowler, *Functional imaging and the central control of the bladder.* J Comp Neurol, 2005. **493**(1): p. 27-32.
40. McDonald, C., K. Winge, and D.J. Burn, *Lower urinary tract symptoms in Parkinson's disease: Prevalence, aetiology and management.* Parkinsonism Relat Disord, 2017. **35**: p. 8-16.
41. Sakakibara, R., et al., *Pathophysiology of bladder dysfunction in Parkinson's disease.* Neurobiol Dis, 2012. **46**(3): p. 565-71.
42. Wolters, A.F., et al., *The TRACK-PD study: protocol of a longitudinal ultra-high field imaging study in Parkinson's disease.* BMC Neurol, 2020. **20**(1): p. 292.
43. Nixon, A., et al., *A validated patient reported measure of urinary urgency severity in overactive bladder for use in clinical trials.* J Urol, 2005. **174**(2): p. 604-7.

44. Goetz, C.G., et al., *Movement Disorder Society-sponsored revision of the Unified Parkinson's Disease Rating Scale (MDS-UPDRS): scale presentation and clinimetric testing results.* Mov Disord, 2008. **23**(15): p. 2129-70.
45. BrainVoyager. *Slice Scan Time Correction*. 11 July 2024 2023; Available from: https://www.brainvoyager.com/bv/doc/UsersGuide/Preprocessing/SliceScanTimeCorrection.html.
46. BrainVoyager. *Motion Detection and Correction*. 2023 11 July 2024]; Available from: https://www.brainvoyager.com/bv/doc/UsersGuide/Preprocessing/MotionDetectionAndCorrection.html.
47. BrainVoyager. *Temporal High-Pass Filtering*. 2014 11 July 2024]; Available from: https://www.brainvoyager.com/bvqx/doc/UsersGuide/Preprocessing/TemporalHighPassFiltering.html.
48. Jezzard, P. and R.S. Balaban, *Correction for geometric distortion in echo planar images from B0 field variations.* Magn Reson Med, 1995. **34**(1): p. 65-73.
49. Inovation, B. *EPI distortion correction: COPE plugin*. 2024 11 July 2024]; Available from: https://support.brainvoyager.com/brainvoyager/available-tools/86-available-plugins/62-epi-distortion-correction-cope-plugin.
50. BrainVoyager. *VMR General Commands*. 2020 11 July 2024]; Available from: https://download.brainvoyager.com/bv/doc/PythonGuide/Scripting/VMRGeneralCommands.html.
51. BrainVoyager. *Preparatory Steps*. 2023 11 July 2024]; Available from: https://www.brainvoyager.com/bv/doc/UsersGuide/Segmentation/PreparatorySteps.html.
52. BrainVoyager. *Intensity Inhomogeneity Correction*. 2023 11 July 2024]; Available from: https://www.brainvoyager.com/bv/doc/UsersGuide/Segmentation/IntensityInhomogeneityCorrection.html.
53. BrainVoyager. *VMR-VTC Commands*. 2020 11 July 2024]; Available from: https://download.brainvoyager.com/bv/doc/PythonGuide/Scripting/VMRVTCCommands.html.
54. MathWorks. *imregtform*. 2024 11 July 2024]; Available from: https://nl.mathworks.com/help/images/ref/imregtform.html#d126e187274.
55. MathWorks. *imregister*. 2024 11 July 2024]; Available from: https://nl.mathworks.com/help/images/ref/imregister.html.
56. Keren, N.I., et al., *In vivo mapping of the human locus coeruleus.* Neuroimage, 2009. **47**(4): p. 1261-7.
57. Blanco, L., et al., *Critical evaluation of the anatomical location of the Barrington nucleus: relevance for deep brain stimulation surgery of pedunculopontine tegmental nucleus.* Neuroscience, 2013. **247**: p. 351-63.
58. Manohar, A., et al., *Brainstem network dynamics underlying the encoding of bladder information.* eLife, 2017. **6**: p. e29917.
59. Curtis, A.L., et al., *Activation of the locus coeruleus noradrenergic system by intracoerulear microinfusion of corticotropin-releasing factor: effects on discharge rate, cortical norepinephrine levels and cortical electroencephalographic activity.* J Pharmacol Exp Ther, 1997. **281**(1): p. 163-72.
60. Gernone, F., et al., *A review of the neural control of micturition in dogs and cats: neuroanatomy, neurophysiology and neuroplasticity.* Vet Res Commun, 2022. **46**(4): p. 991-998.
61. Gawryluk, J.R., E.L. Mazerolle, and R.C. D'Arcy, *Does functional MRI detect activation in white matter? A review of emerging evidence, issues, and future directions.* Front Neurosci, 2014. **8**: p. 239.
62. Ding, Z., et al., *Spatio-temporal correlation tensors reveal functional structure in human brain.* PLoS One, 2013. **8**(12): p. e82107.

63. Tettamanti, M., et al., *Interhemispheric transmission of visuomotor information in humans: fMRI evidence.* J Neurophysiol, 2002. **88**(2): p. 1051-8.
64. Habas, C. and M. Manto, *Probing the neuroanatomy of the cerebellum using tractography.* Handb Clin Neurol, 2018. **154**: p. 235-249.
65. Haines, D.E., *Neuroanatomy in clinical context : an atlas of structures, sections, systems, and syndromes*. 9th edition ed. 2015, Philadelphia: Wolters Kluwer Health.
66. Bastide, L. and A.G. Herbaut, *Cerebellum and micturition: what do we know? A systematic review.* Cerebellum Ataxias, 2020. **7**: p. 9.
67. Bradley, W.E. and C.T. Teague, *Cerebellar influence on the micturition reflex.* Exp Neurol, 1969. **23**(3): p. 399-411.
68. Martner, J., *Influences on the defecation and micturition reflexes by the cerebellar fastigial nucleus.* Acta Physiol Scand, 1975. **94**(1): p. 95-104.
69. Nishizawa, O., et al., *Effect of cerebellectomy on reflex micturition in the decerebrate dog as determined by urodynamic evaluation.* Urol Int, 1989. **44**(3): p. 152-6.
70. Nour, S., et al., *Cerebral activation during micturition in normal men.* Brain, 2000. **123 (Pt 4)**: p. 781-9.
71. Athwal, B.S., et al., *Brain responses to changes in bladder volume and urge to void in healthy men.* Brain, 2001. **124**(Pt 2): p. 369-77.
72. Blok, B.F., L.M. Sturms, and G. Holstege, *A PET study on cortical and subcortical control of pelvic floor musculature in women.* J Comp Neurol, 1997. **389**(3): p. 535-44.
73. Tateno, F., et al., *Lower Urinary Tract Function in Spinocerebellar Ataxia 6.* Low Urin Tract Symptoms, 2012. **4**(1): p. 41-4.
74. Pea, U., et al., *Vesico-sphincter dysfunctions in Pure Cerebellar Syndrome (PCS): a possible basis for the study of anatomo-functional correlations.* Urologia, 2008. **75**(1): p. 38-41.
75. Dietrichs, E. and D.E. Haines, *Possible pathways for cerebellar modulation of autonomic responses: micturition.* Scand J Urol Nephrol Suppl, 2002(210): p. 16-20.
76. Al-Chalabi, M., V. Reddy, and I. Alsalman, *Neuroanatomy, Posterior Column (Dorsal Column)*, in *StatPearls*. 2024, StatPearls Publishing

Copyright © 2024, StatPearls Publishing LLC.: Treasure Island (FL) ineligible companies. Disclosure: Vamsi Reddy declares no relevant financial relationships with ineligible companies. Disclosure: Ihsan Alsalman declares no relevant financial relationships with ineligible companies.

77. Navarro-Orozco, D. and P.C. Bollu, *Neuroanatomy, Medial Lemniscus (Reils Band, Reils Ribbon)*, in *StatPearls*. 2024, StatPearls Publishing

Copyright © 2024, StatPearls Publishing LLC.: Treasure Island (FL) with ineligible companies. Disclosure: Pradeep Bollu declares no relevant financial relationships with ineligible companies.

78. Hoch, M.J., et al., *3T MRI Whole-Brain Microscopy Discrimination of Subcortical Anatomy, Part 1: Brain Stem.* AJNR Am J Neuroradiol, 2019. **40**(3): p. 401-407.
79. Schott, B., et al., *Is the Brainstem Activation Different Between Healthy Young Male and Female Volunteers at Initiation of Voiding? A High Definition 7-Tesla Magnetic Resonance Imaging Study.* Int Neurourol J, 2023. **27**(3): p. 174-181.
80. Kameyama, M., K. Murakami, and M. Jinzaki, *Comparison of [(15)O] H2O Positron Emission Tomography and Functional Magnetic Resonance Imaging in Activation Studies.* World J Nucl Med, 2016. **15**(1): p. 3-6.
81. Fan, A.P., et al., *Comparison of cerebral blood flow measurement with [15O]-water positron emission tomography and arterial spin labeling magnetic resonance imaging: A systematic review.* J Cereb Blood Flow Metab, 2016. **36**(5): p. 842-61.
82. Zhang, X., et al., *Linear Registration of Brain MRI Using Knowledge-Based Multiple Intermediator Libraries.* Front Neurosci, 2019. **13**: p. 909.

83. Gratzke, C., et al., *EAU Guidelines on the Assessment of Non-neurogenic Male Lower Urinary Tract Symptoms including Benign Prostatic Obstruction.* Eur Urol, 2015. **67**(6): p. 1099-1109.
84. Ranzenberger, L.R., J.M. Das, and T. Snyder, *Diffusion Tensor Imaging*, in *StatPearls*. 2024, StatPearls Publishing

Appendix A

For the scripts used for the preprocessing and post-processing steps, please click this link:

https://github.com/ArmelleKn/Thesis_TM

In this github repository all used scripts are available.

For Python scripts used for preprocessing, see folder: 'Python scripts preprocessing'.

For MATLAB scripts used for post-processing, see folder: 'MATLAB scripts postprocessing'.

Appendix B

Here the first eight examples of the registration of the pons in MNI space are shown before and after usage of the pons registration tool. For all the results of the pons registration tool, see:

https://github.com/ArmelleKn/Thesis_TM --> Results_registration_tool.docx

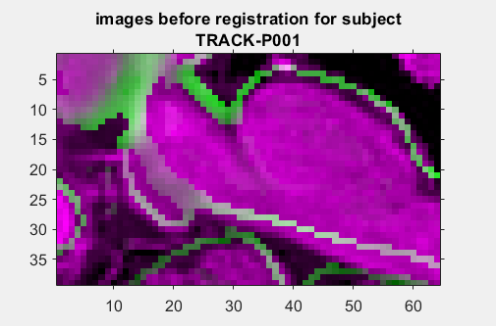

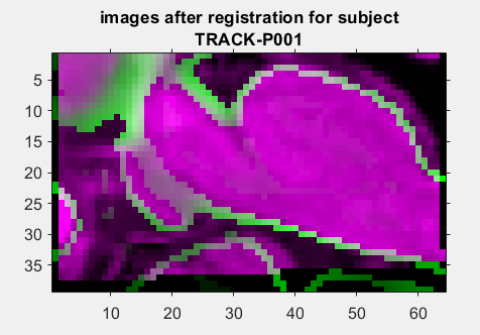

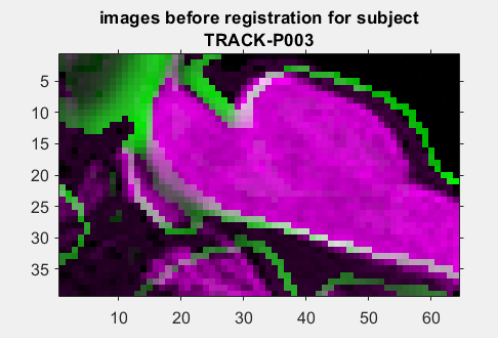

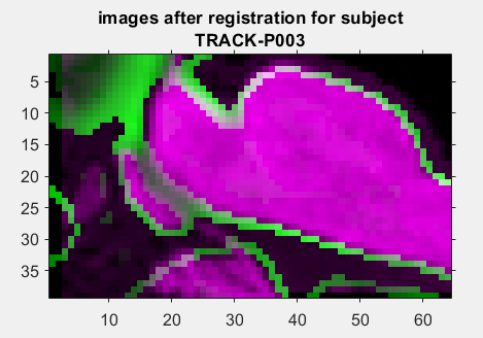

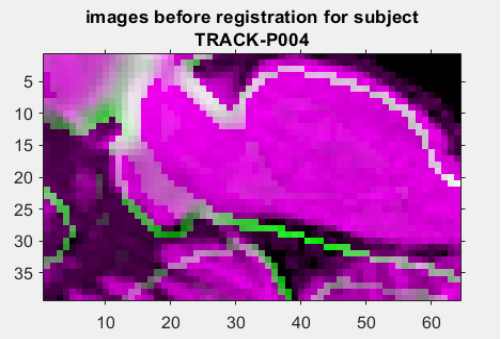

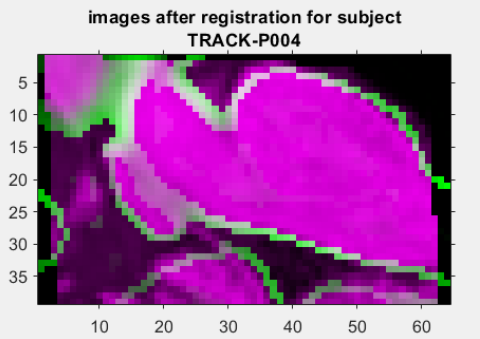

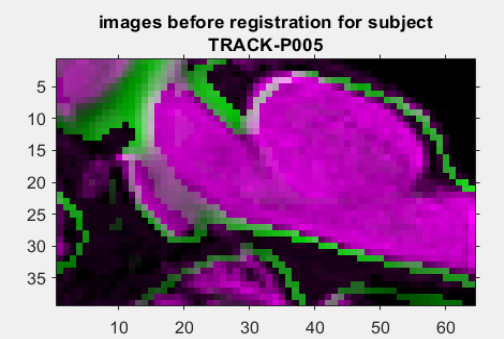

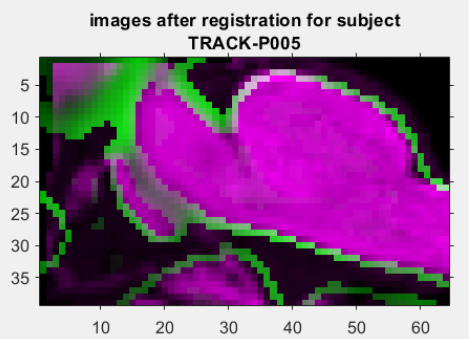

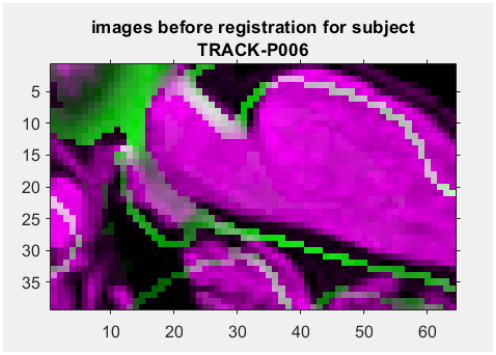
images before registration for subject
TRACK-P006
5
10
15
20
25
30
35
10
20
30
40
50
60

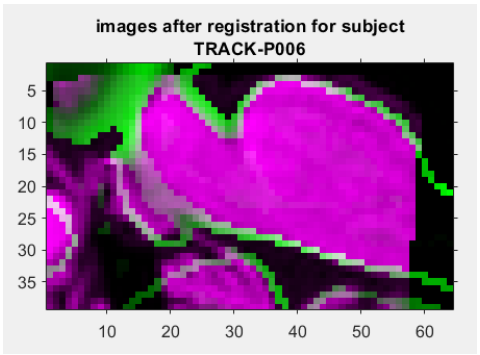
images after registration for subject
TRACK-P006
5
10
15
20
25
30
35
10
20
30
40
50
60

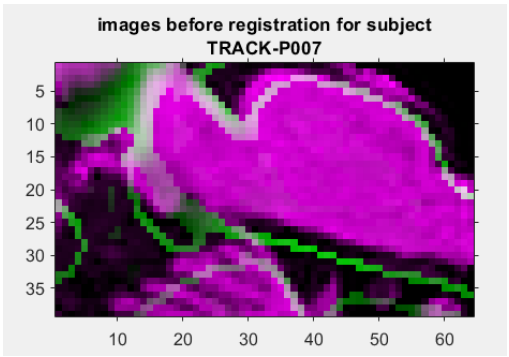
images before registration for subject
TRACK-P007
5
10
15
20
25
30
35
10
20
30
40
50
60

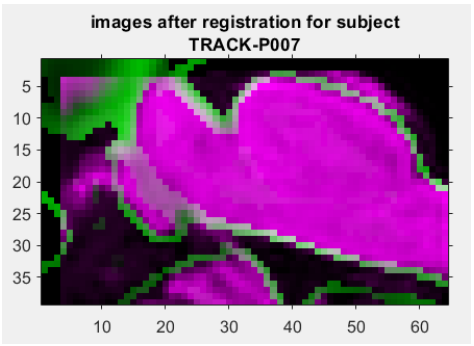
images after registration for subject
TRACK-P007
5
10
15
20
25
30
35
10
20
30
40
50
60

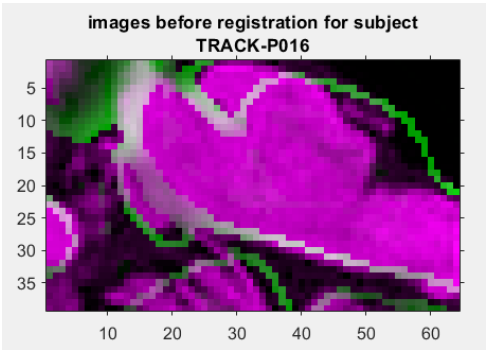
images before registration for subject
TRACK-P016
5
10
15
20
25
30
35
10
20
30
40
50
60

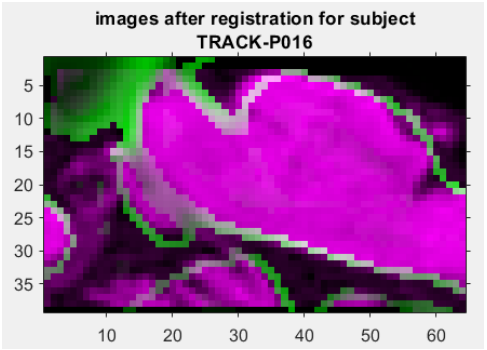
images after registration for subject
TRACK-P016
5
10
15
20
25
30
35
10
20
30
40
50
60

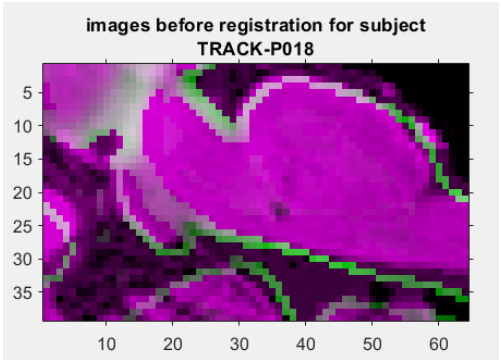
images before registration for subject
TRACK-P018
5
10
15
20
25
30
35
10
20
30
40
50
60

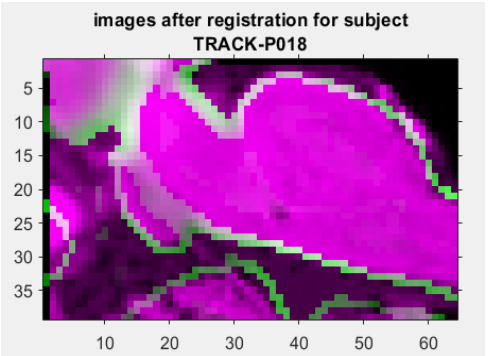
images after registration for subject
TRACK-P018
5
10
15
20
25
30
35
10
20
30
40
50
60